This pdf file consists of all figures and photographs, and their captions, scanned from Chapters 4 and 5 of:

EXPERIMENTAL GROWTH OF FIBERS AND FIBROUS VEINS

by

Taohong Li

A Dissertation

Submitted to the University at Albany, State University of New York

in Partial Fulfillment of

the Requirements for the Degree of

Doctor of Philosophy

College of Arts & Sciences

Department of Earth & Atmospheric Sciences

2000

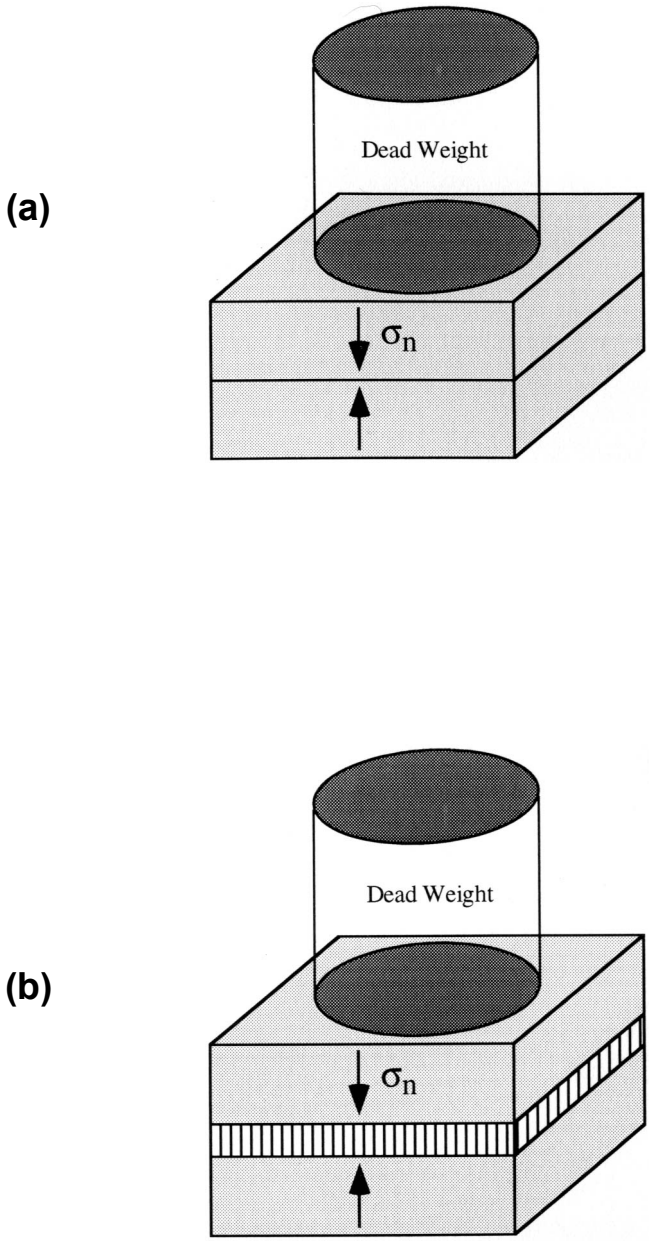

Fig. 4.1 Set-up for growth of fibrous veins under dead-weight loading. (**a**) Initial state of sample. A dead weight is placed on top of two superimposed ceramic blocks which are soaked with a crystallizing fluid and are coated with epoxy except on the crack side between them. (**b**) A fibrous vein grows between the blocks by lifting the upper block and the dead weight. Length and thickness of ceramic block are about 2 cm and 5 mm, respectively.

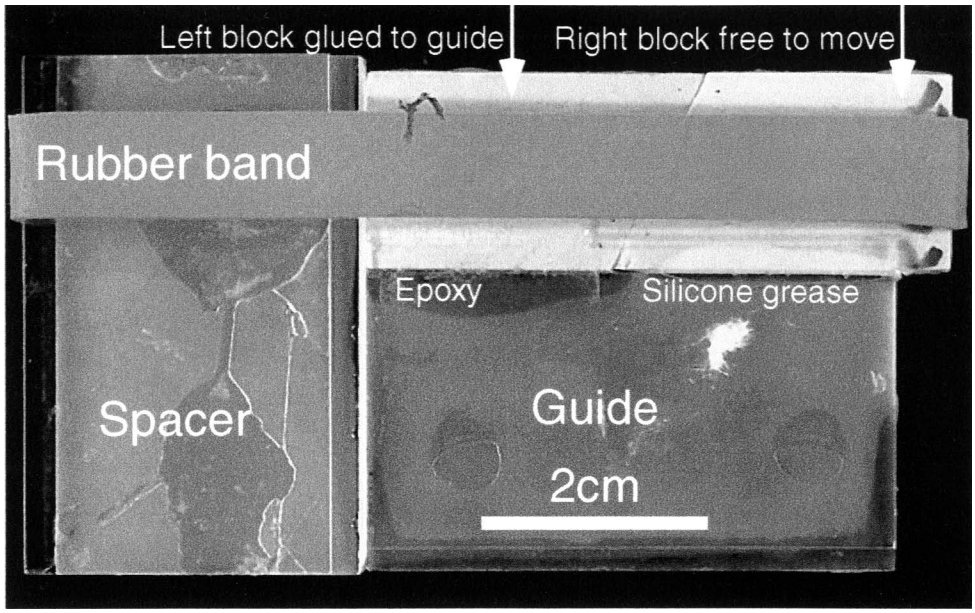

Fig. 4.2 Set-up for growth of fibrous veins under rubber-band loading. Of the two analog wall blocks (porous ceramic), the left one is cemented on the guide with epoxy while the right one is free to move on silicone grease. A compressive loading is imposed on the blocks by means of a rubber band. The spacer on the left is simply used to stretch the rubber band to create a desirable amount of compressive force. The ceramic blocks are coated with epoxy except on the crack side and are saturated with the crystallizing solution of NH_4SCN or N_aNO_3 at the beginning of experiment. Crystallization and vein opening occur at the crack as the result of evaporation of water from the pore fluid at the crack.

Fig. 4.3 Photographs showing progressive opening of a vein of fibers of NH_4SCN under a dead weight of 320 grams (0.12 bars) in experiment *DW-01*. Ceramic blocks were coated with epoxy except on the vein side and growth occurred in a closed desiccator with an ambient relative humidity of about 10%. Number in the upper-right corner of each picture represents the time interval of the corresponding growth stage. To show the progressive vein dilations and upward liftings through the stages, the photographs are aligned such that the lower block is fixed with respect to the picture.

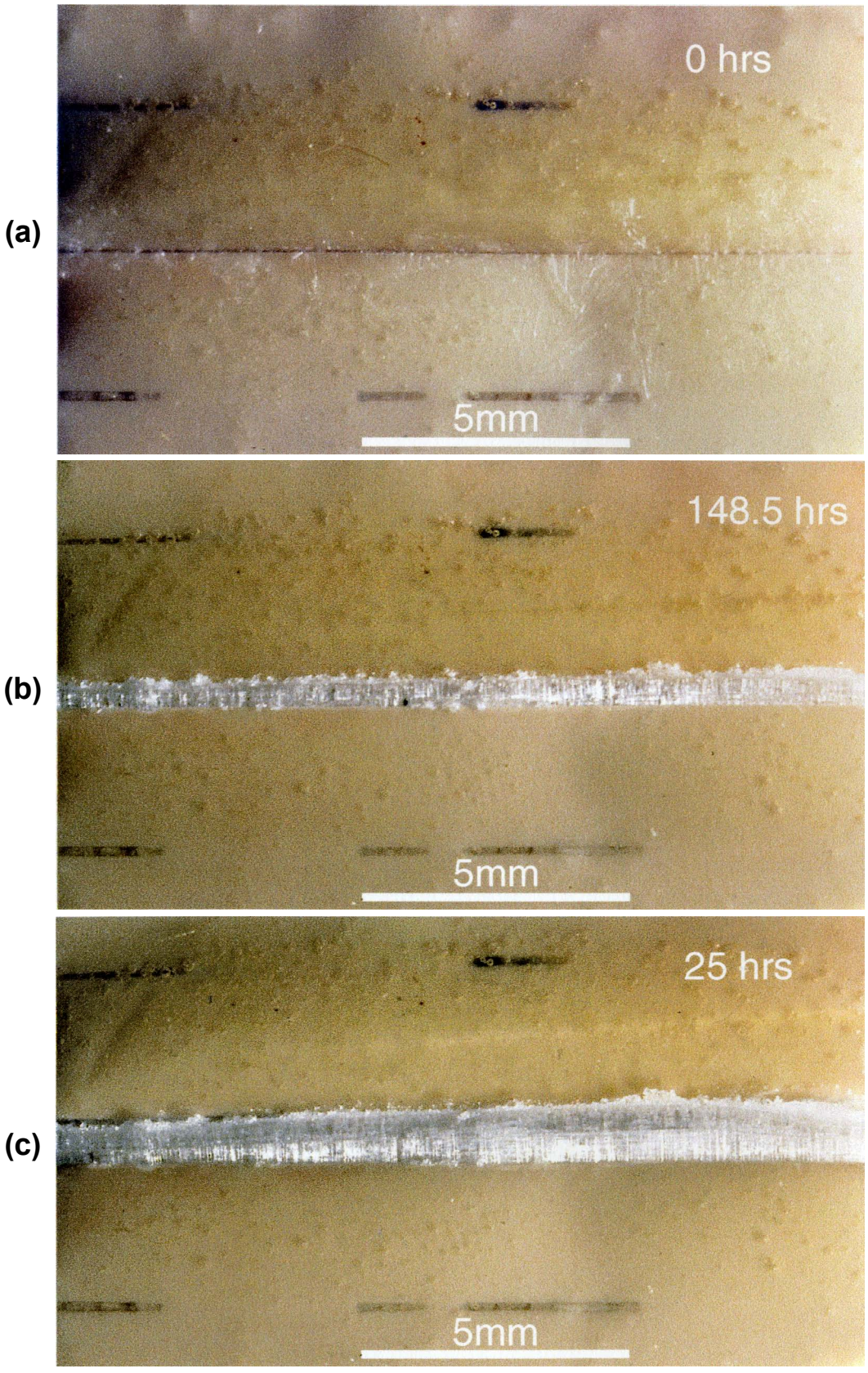
(a)
0 hrs
5mm
(b)
148.5 hrs
5mm
(c)
25 hrs
5mm

(d)

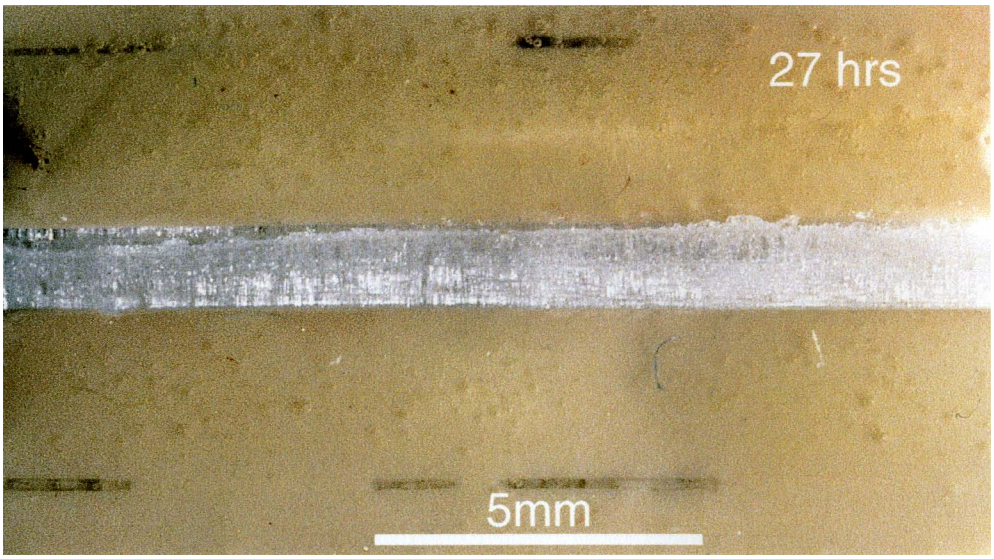

(e)

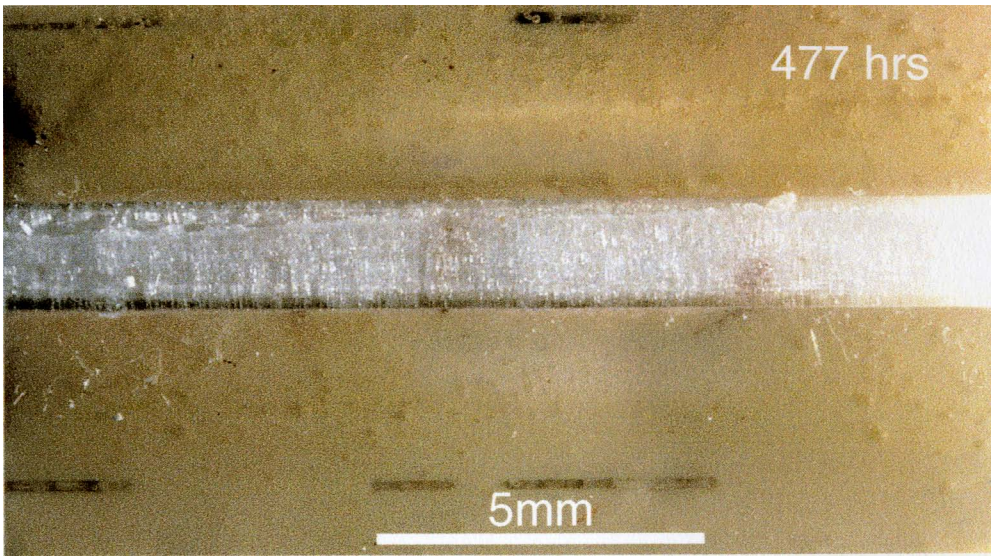

Fig. 4.4 Growth of a vein of fibers of NH_4SCN under a dead weight of 1160 grams (0.88 bars) in experiment *DW-02*. Ceramic blocks were coated with epoxy except on the vein side and growth occurred in a closed desiccator with an ambient relative humidity of about 10%. (**a**) Initial crack between the blocks. (**b**) A vein of tightly-packed fibers forced open by fiber growth as seen 50 days later. The two sides of the vein are also tightly welded and no clear median suture is visible. (**c**) & (**d**) An enlarged view of the vein showing tightly packed character of fibers and continuity of at least some fibers from one side to the other (arrow).

(a)

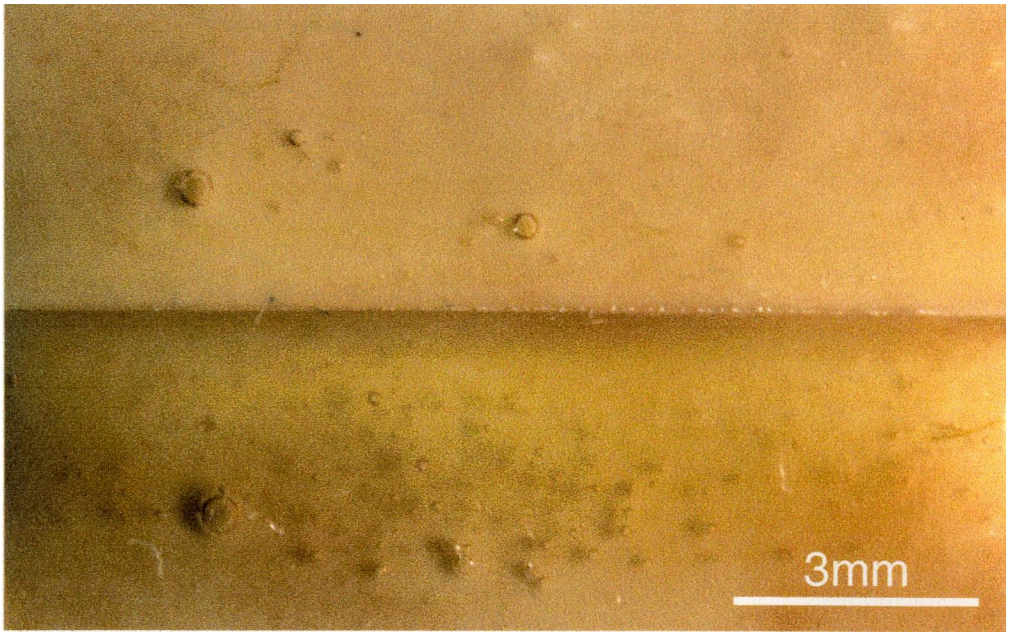

(b)

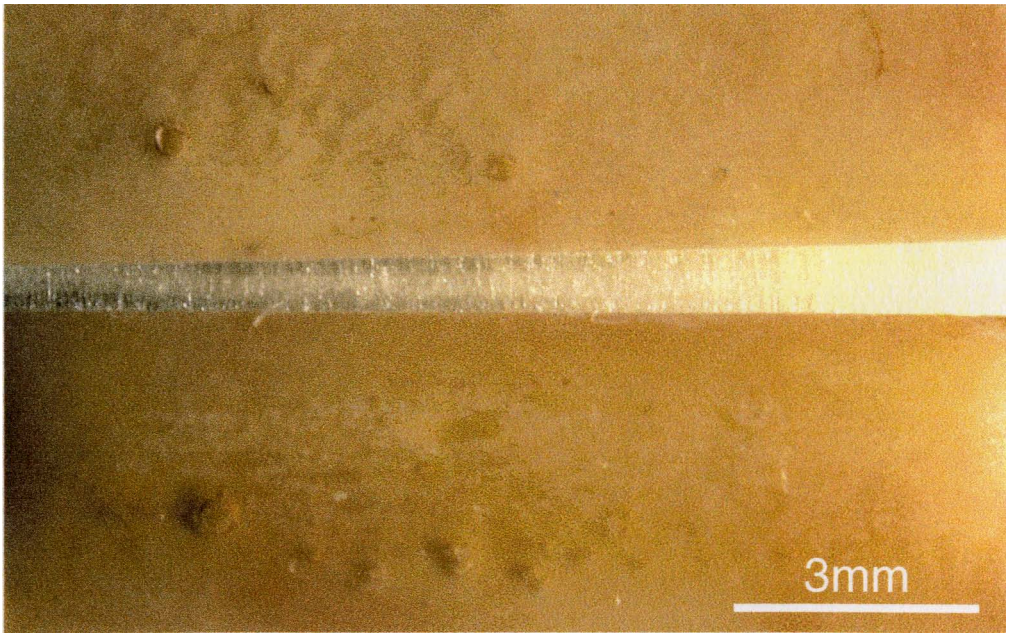

(c)

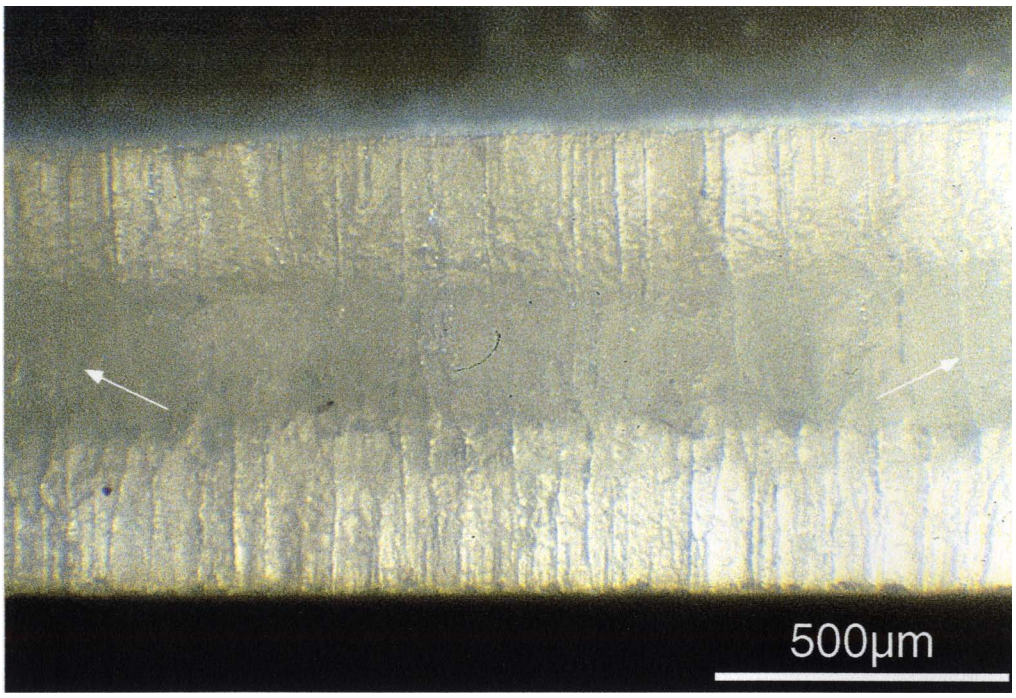

(d)

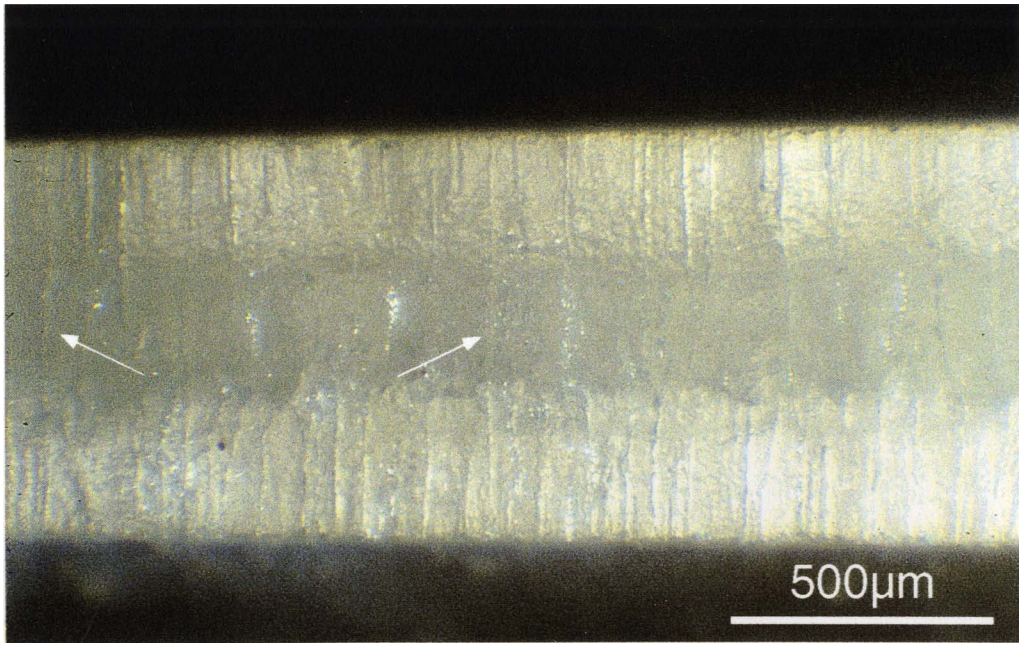

Fig. 4.5 Growth of a vein of fibers of NH_4SCN under a dead weight of 2200 grams (1.3 bars) in experiment *DW-08*. Ceramic blocks were painted black and coated with epoxy except on the vein side and growth occurred in a closed desiccator with an ambient relative humidity of about 10%. (**a**) Initial growth of a thin seam of fibers on the 7th day of the experiment. (**b**) A widely dilated vein of tightly-packed transparent fibers as seen on the 28th day of the experiment. The two sides of the vein are tightly welded and the median suture is not well-defined. (**c**) An enlarged view of the vein on the 54th day of the experiment showing good, tightly packed quality of fibers. No median suture is clearly visible except some pronounced type I features across the fibers.

(a)

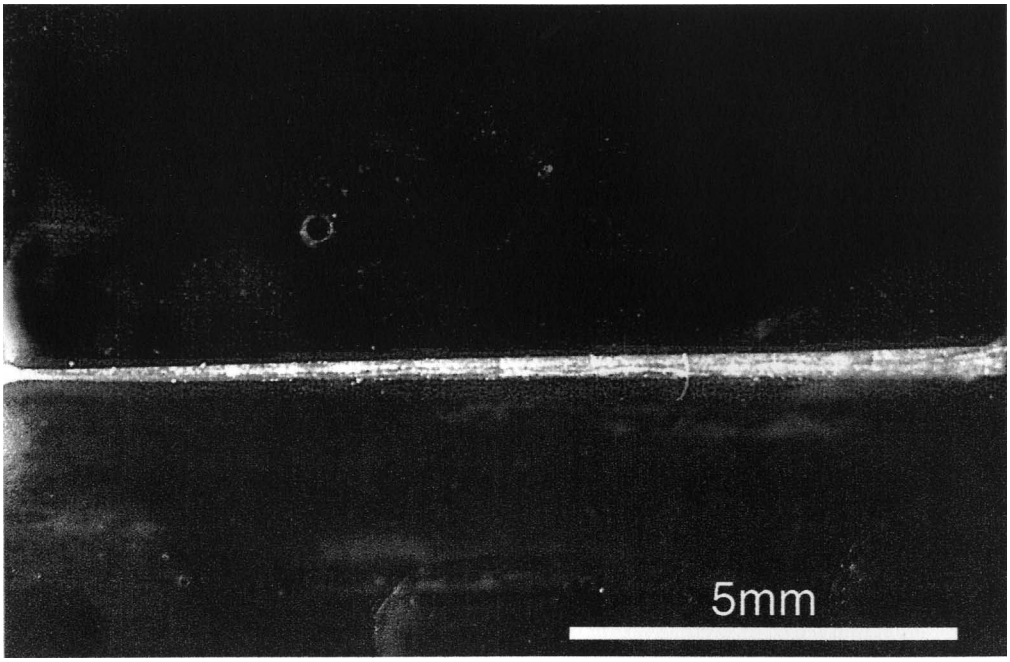

(b)

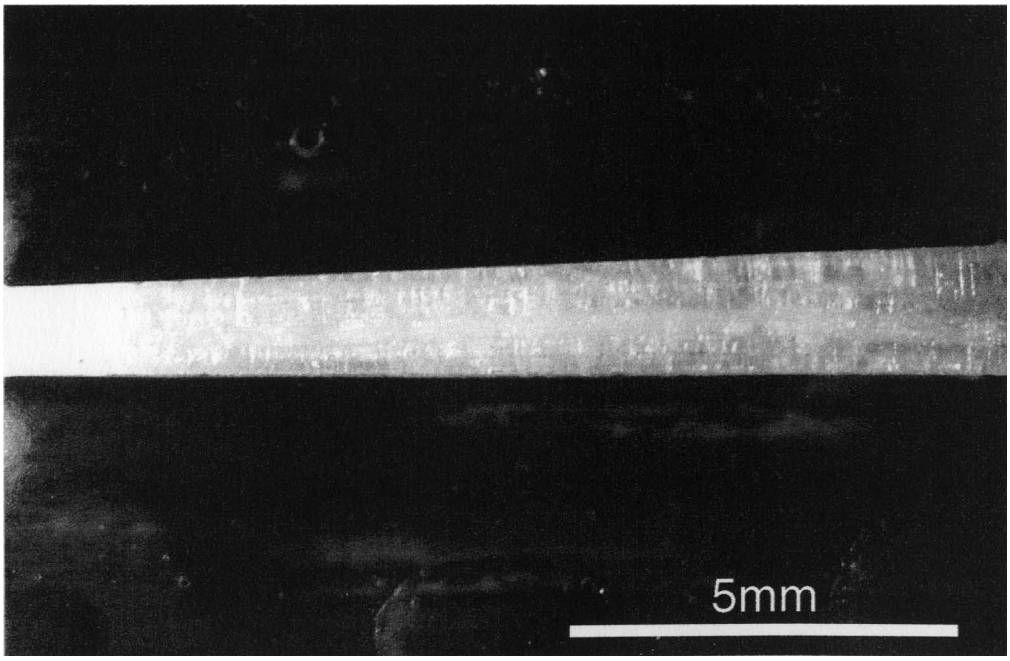

(c)

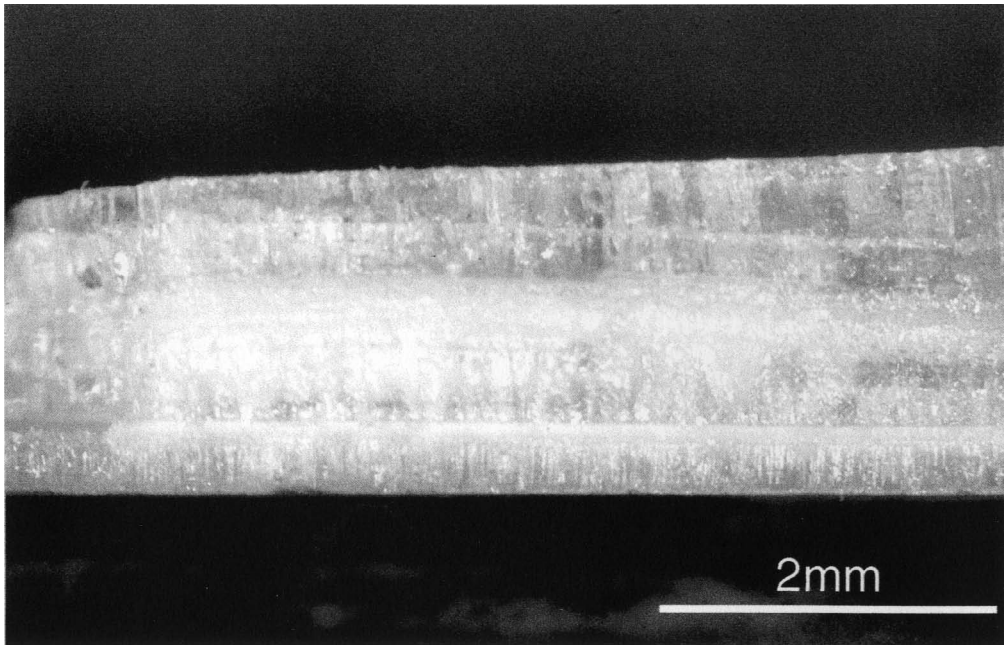

Fig. 4.6 Veins of tightly-packed fibers grown in dead-weight loading experiments. (**a**) A vein of clear, tightly-packed fibers of N_aNO_3 grown under a dead weight of 7.9 kg (2.94 bars) in experiment *DW-17* over a period of 66 days. Some wall-derived fragments can be seen in the middle of the vein. (**b**) A vein of fibers of N_aNO_3 grown under a dead weight of 4 kg (1.57 bars) in experiment *DW-18* over a period of 66 days. A median suture can be seen at the center of the vein. (**c**) A vein of fibers of NH_4SCN grown under a dead weight of 1.5 kg (0.48 bars) in experiment *DW-09* over a period of 15 days. A median suture is visible at the center of the vein.

(a)

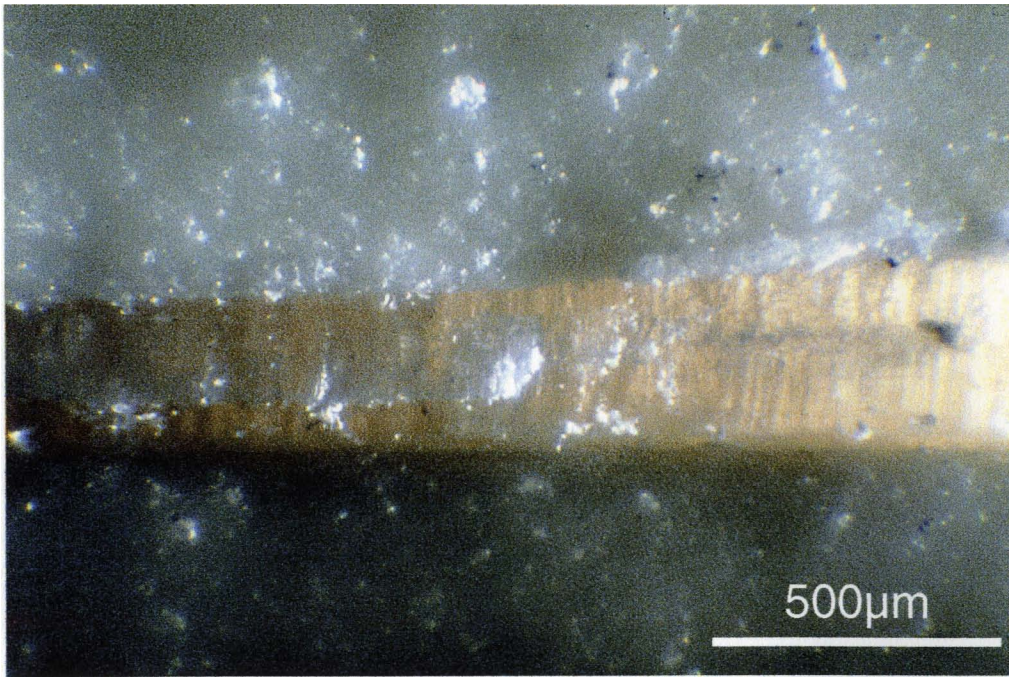

(b)

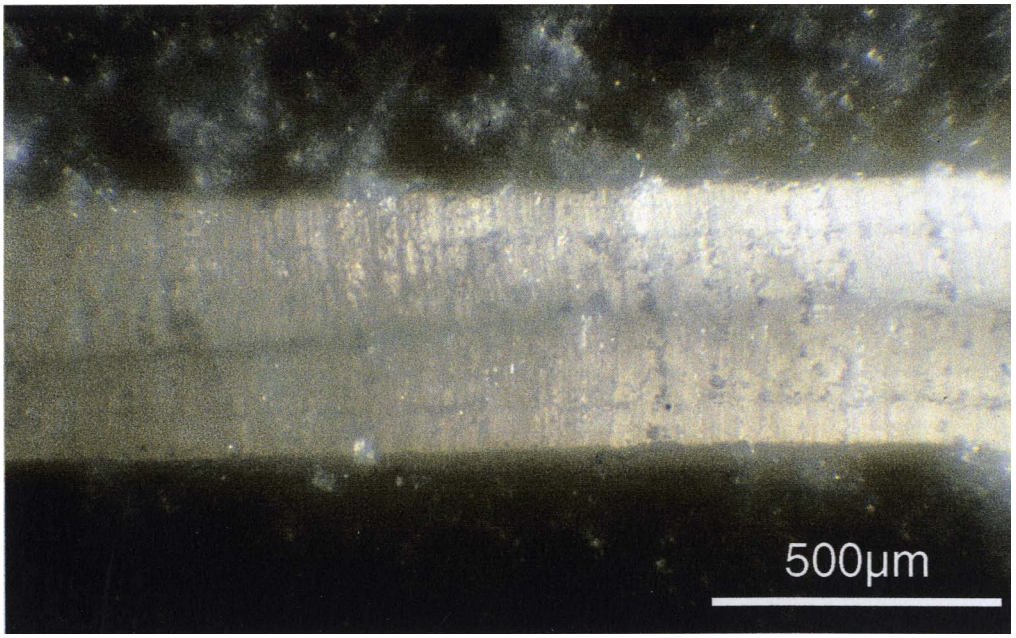

(c)

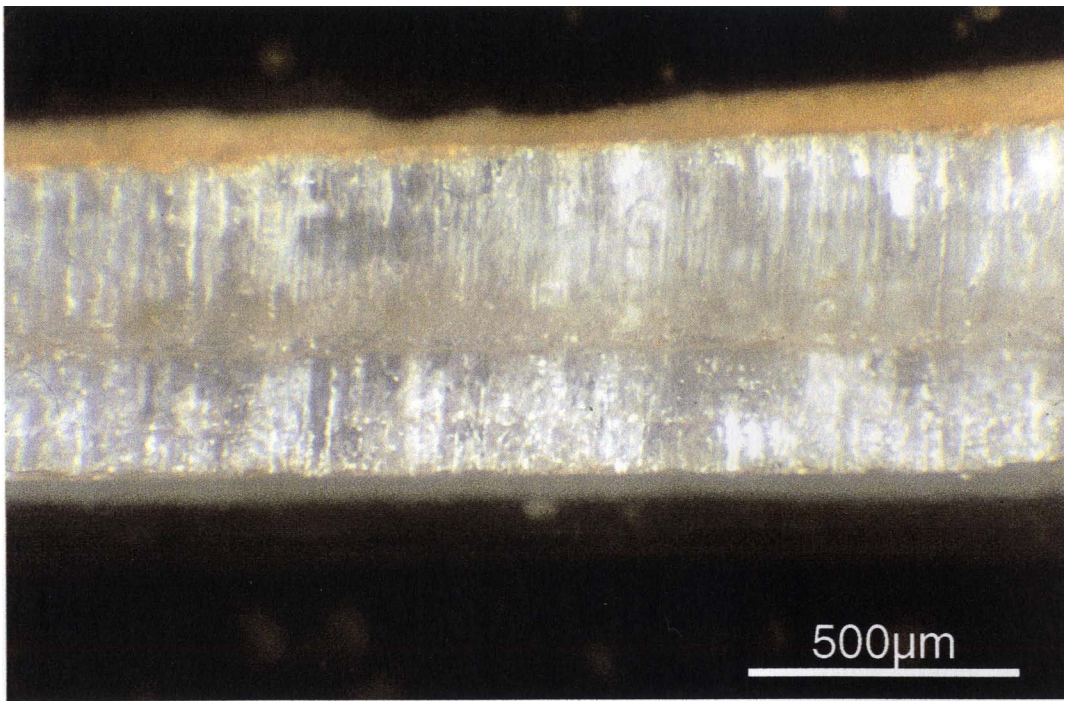

Fig. 4.7 Growth of a vein of fibers of N_aNO_3 under increasing dead-weight loading in experiment *DW-14*.
(**a**) Growth during the first stage of 7 days, against a loading that imposed a pressure of 0.42 bars on the wall blocks. The vein has an asymmetric geometry showing a wider lower half vein than the upper half. The two sides are separated by a marked median suture. (**b**) An enlarged view of part of the same vein.
(**c**) Another view of the same vein on another side of sample of *DW-14* (side c) seen at the end of the first stage of experiment showing the appearance of the vein at this site just before the dead-weight loading was increased. (**d**) View of the same site (with the lower block fixed) 16 days after the loading pressure was increased from 0.42 to 5.7 bars, showing a much widened vein consisting of old fibers (**O**) followed by younger fresh fibers (**Y**) grown against the increased pressure on the wall blocks during the second stage of experiment.
(**e**) Still another view of the same vein on another side of sample (side b) showing the appearance of the vein at this site at the end of the first stage of experiment. (**f**) view of the same site (with the lower block fixed) 16 days after the pressure increase, showing a widened vein consisting of old broken fibers followed by younger fresh fibers grown against the increased pressure during the second stage of experiment. Old fibers were broken as the vein was partly collapsed by the sudden increase of pressure at the beginning of the second stage. New growth under the increased pressure has mainly occurred on the side of the upper block. Red patches are pen ink markers placed on the vein just before the increase of the loading.
(**g**) Enlarged view of the new fibers grown at the site of (d) against the increased pressure during the second stage of experiment. After this picture was taken, the dead-weight loading was further increased to 8.3 bars during the third stage of experiment. (**h**) The appearance of the fibers at the same site as seen 11 days later. There is clearly more growth (**N**) that occurred under the newly increased pressure during this period although its thickness is very small. Note that there is a marked Type I discontinuity across the fibers grown during the 2nd stage.
(**i**) Another view of old fibers broken and new fibers grown during the second stage of experiment, seen before the dead-weight loading pressure was increased to 8.3 bars for the third stage of experiment. (**j**) The same view as seen 11 days later at the same scale. The green color of the fibers and the wall was imparted by the green marker pen immediately before the loading increase. The thickness of the fresh fiber growth has clearly increased under the increased pressure during the third stage of experiment.

(a)

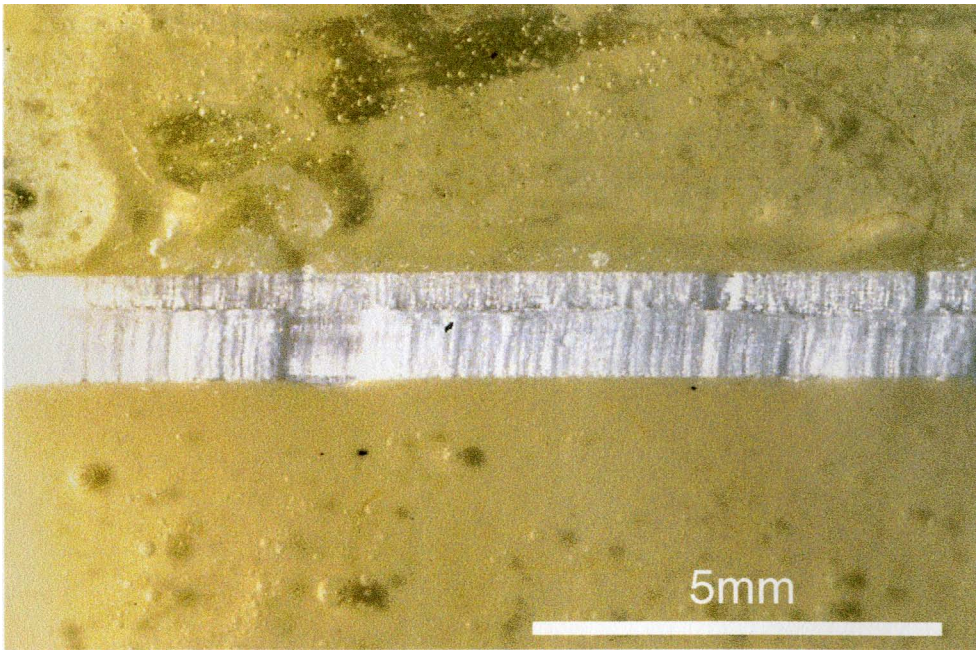

(b)

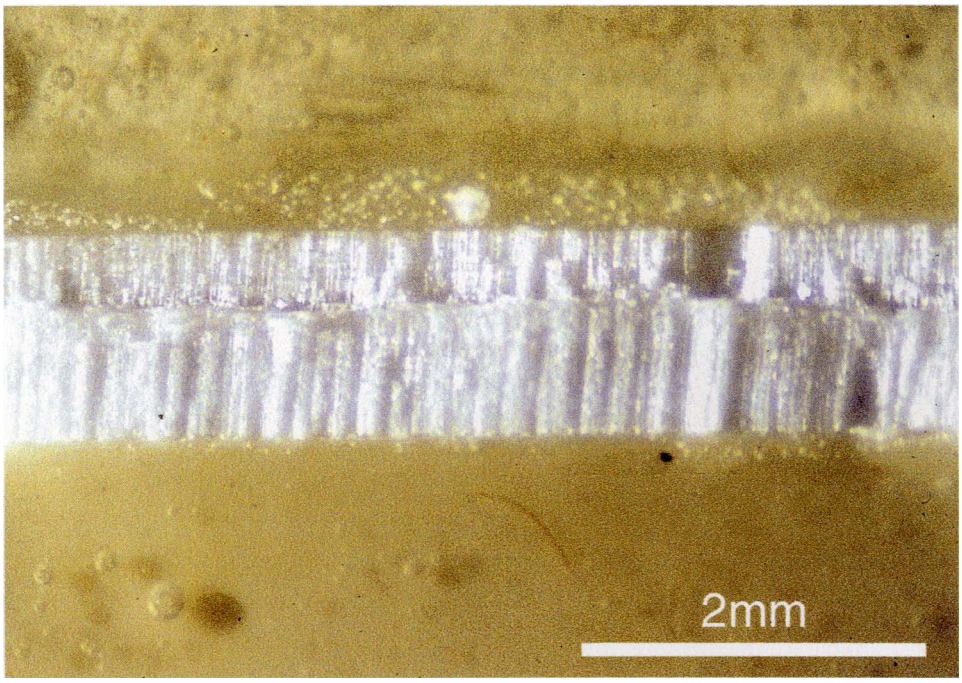

(c)

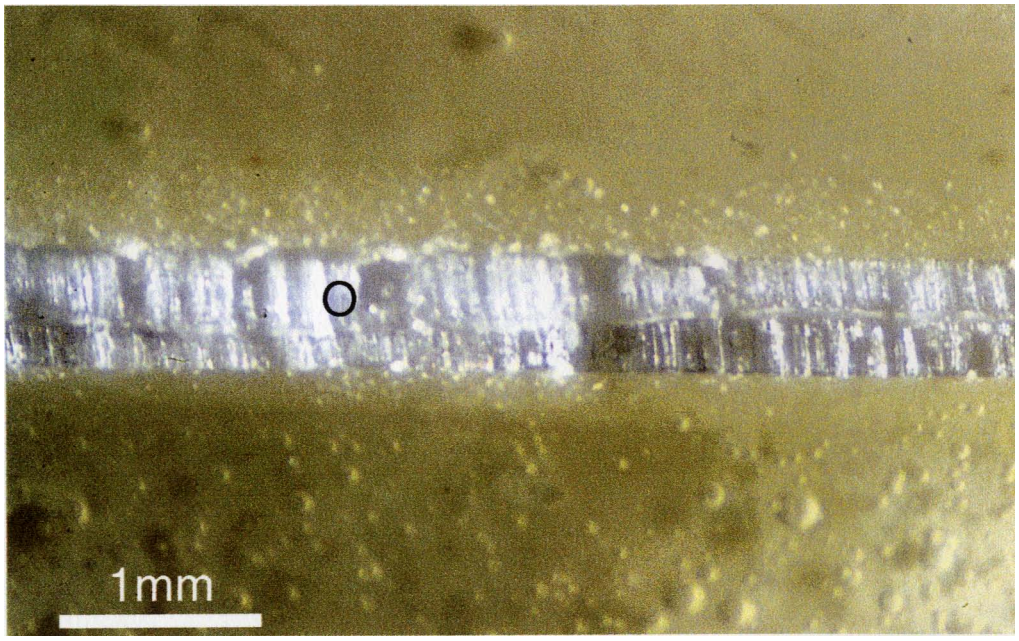

(d)

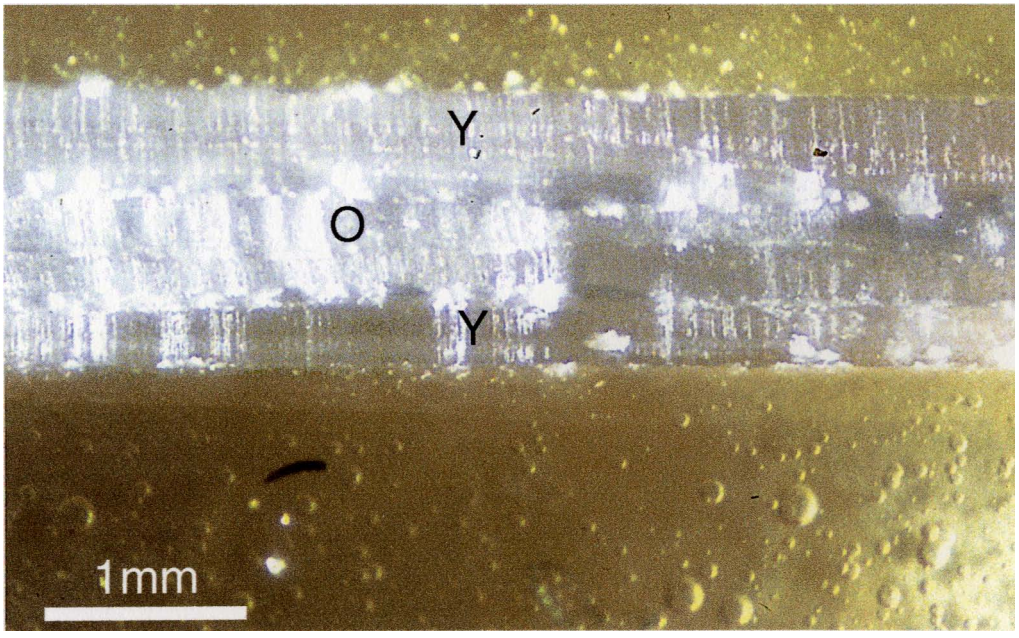

(e)

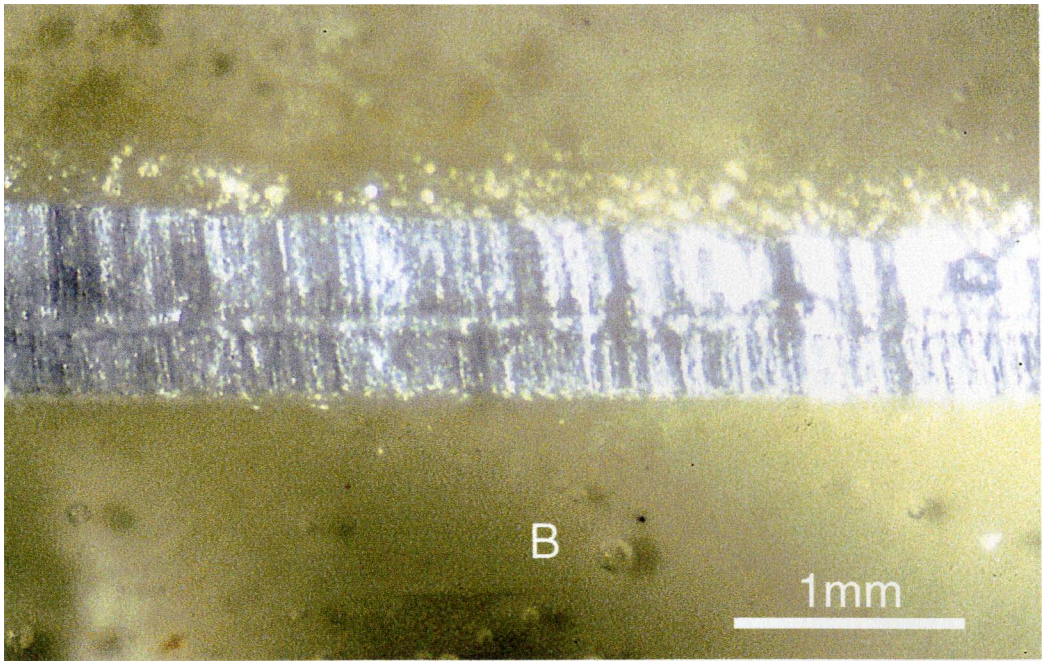

(f)

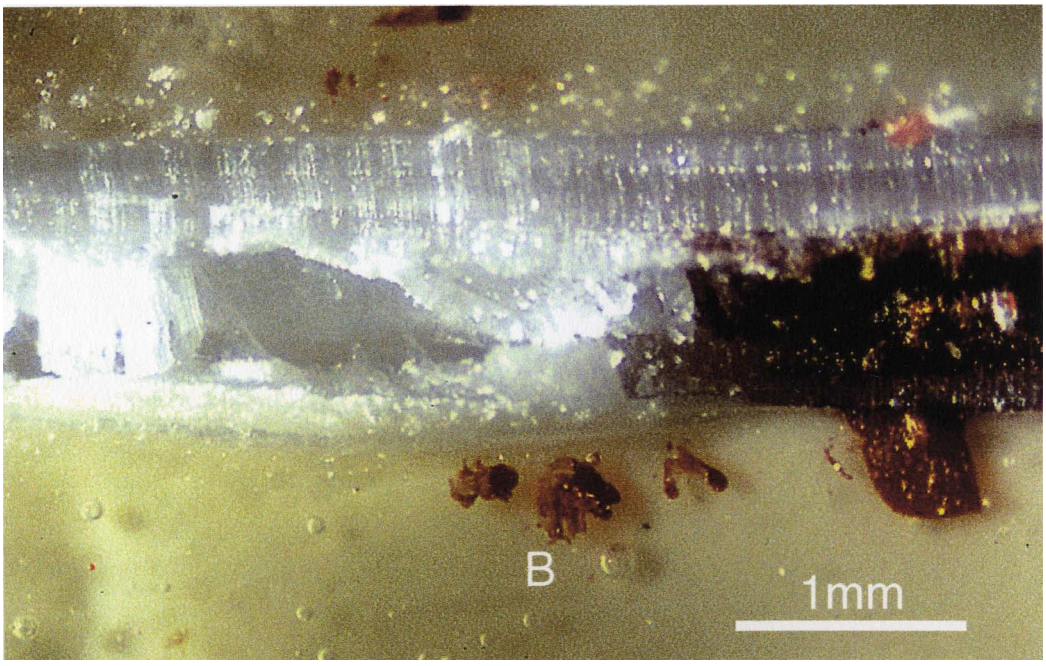

(g)

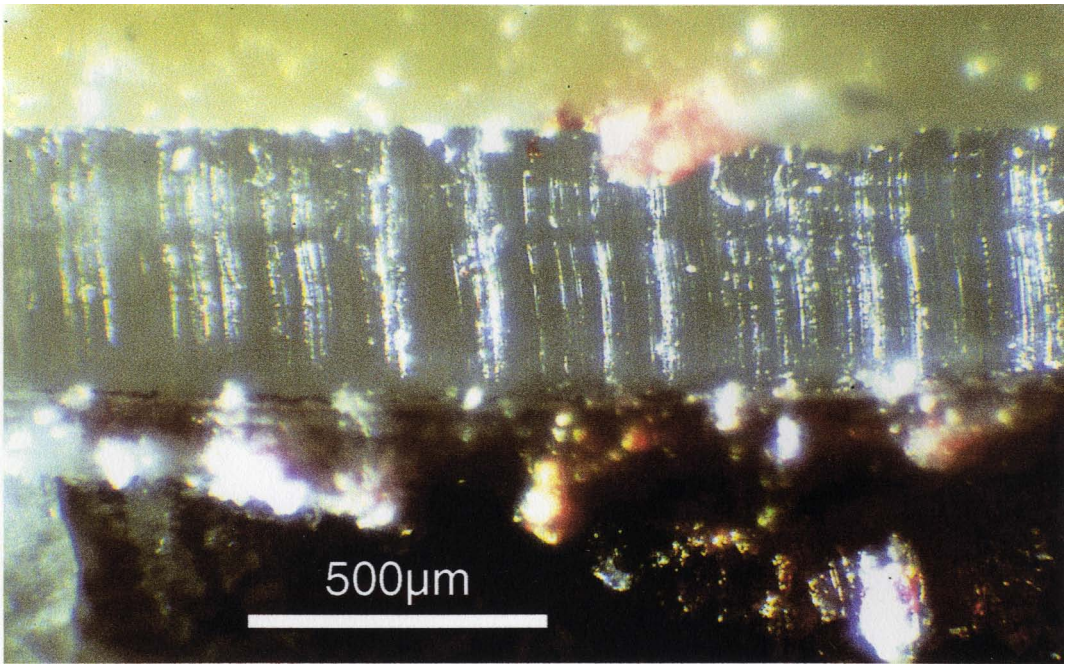

(h)

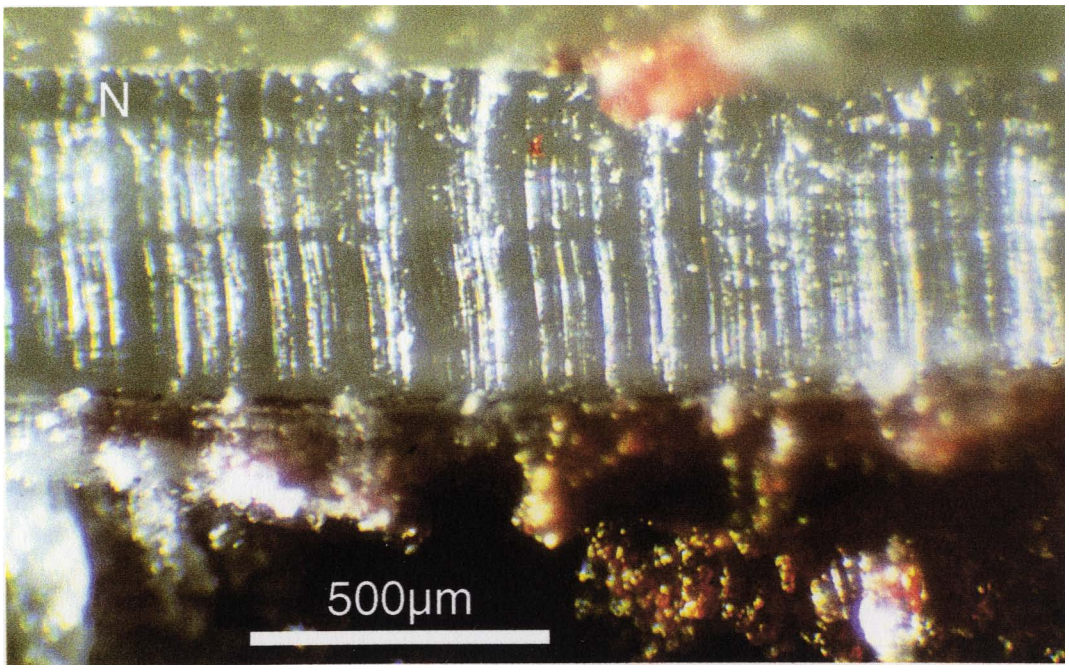

(i)

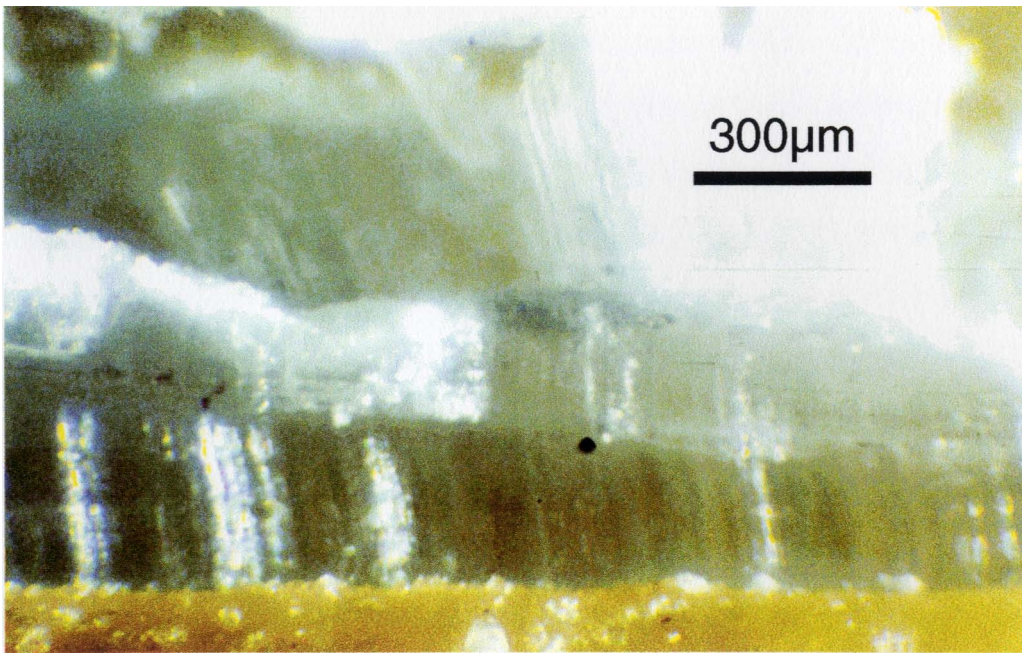

(j)

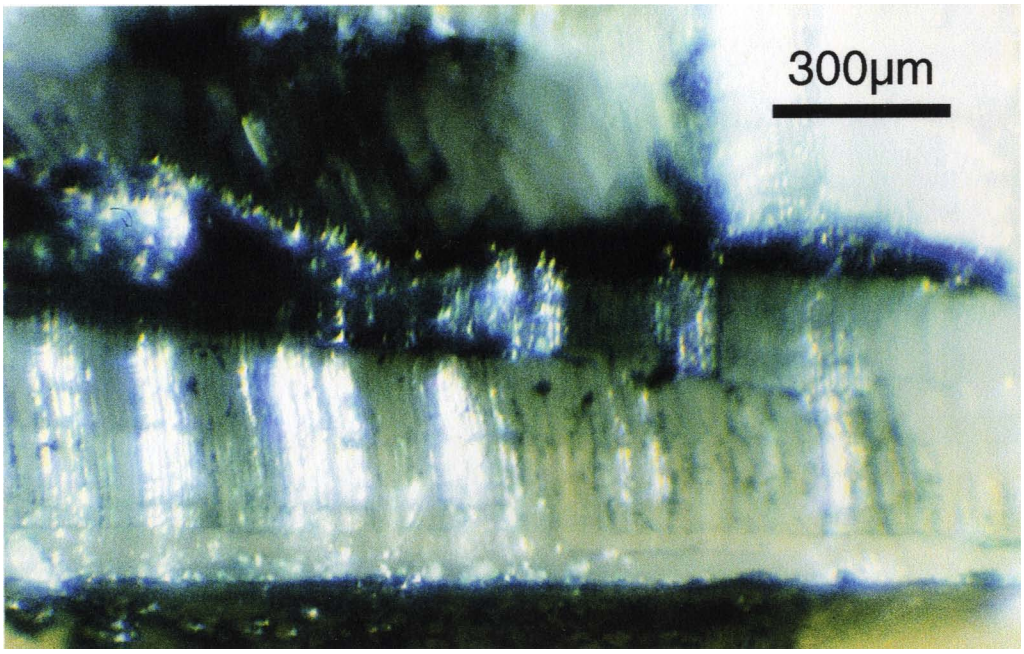

Fig. 4.8 Growth of a vein of fibers of N_aNO_3 under increasing dead-weight loading in experiment *DW-13*.
(**a**) Growth during the first stage of 6 days, against a dead-weight loading pressure of 0.42 bars on the wall blocks. The vein has an asymmetric geometry showing a wider lower half vein than the upper half.
(**b**) View of part of the same vein marked with pen ink. After this picture was taken, the loading pressure on the sample was increased to 16.6 bars.
(**c**) Photograph of the collapsed vein, taken 7 days after the loading pressure was increased.
(**d**) Photograph of the collapsed vein on another side of sample (side c), taken 7 days after the pressure increase, showing some fresh fibers grown from the lower wall into the collapsed vein, with or without accompanying vein dilation.
(**e**) Photograph of a new vein of curved fibers developed in one of the fractured epoxy-coated ceramic blocks, as seen 7 days after the pressure increase. The curved morphology of fibers indicates that the vein must have been forced open as fibers were growing, thus forming a typical vein of synkinematic growth.
(**f**) Photograph of one end of the collapsed vein showing fiber growth on fracture surfaces (F) and new vein growth (V) in the fractured wall blocks.

(a)

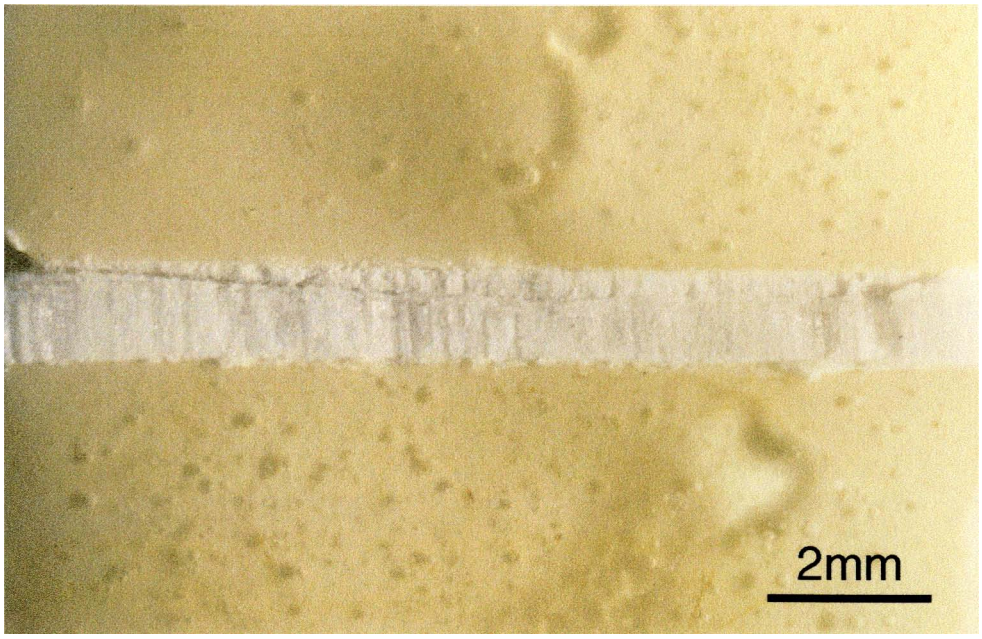

(b)

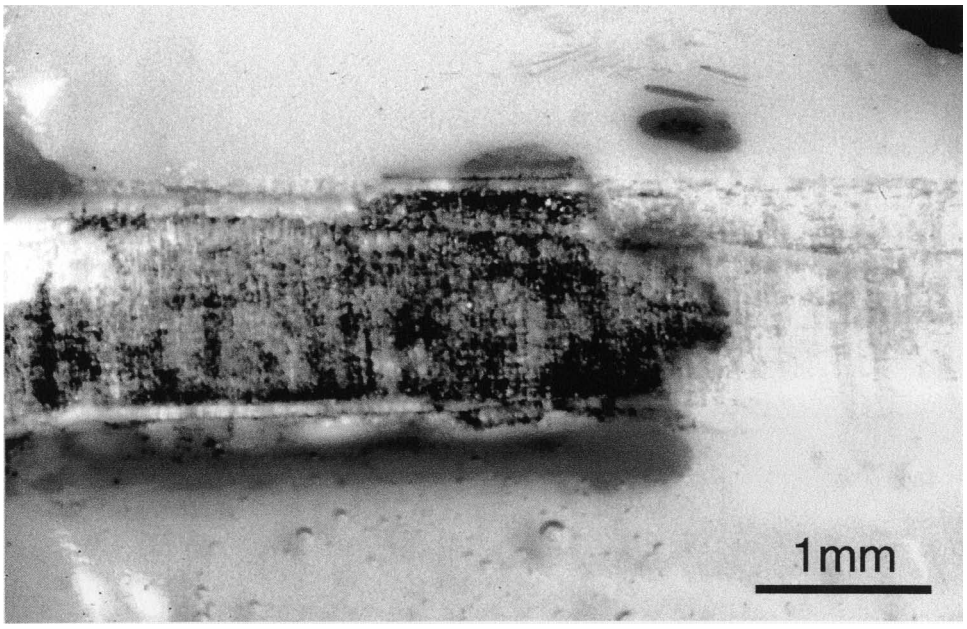

(c)

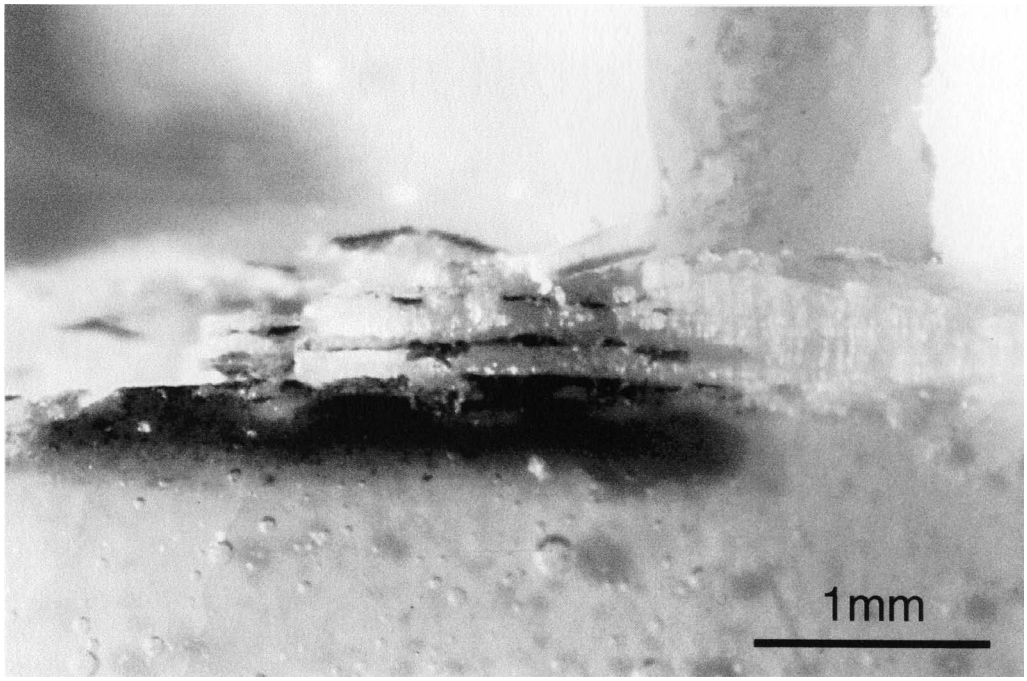

(d)

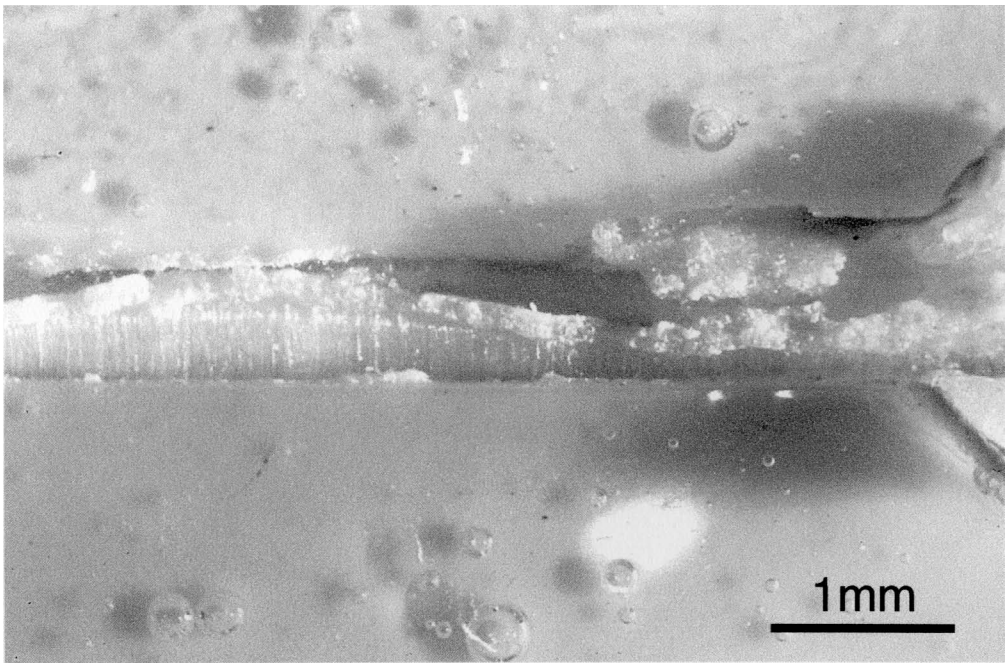

(e)

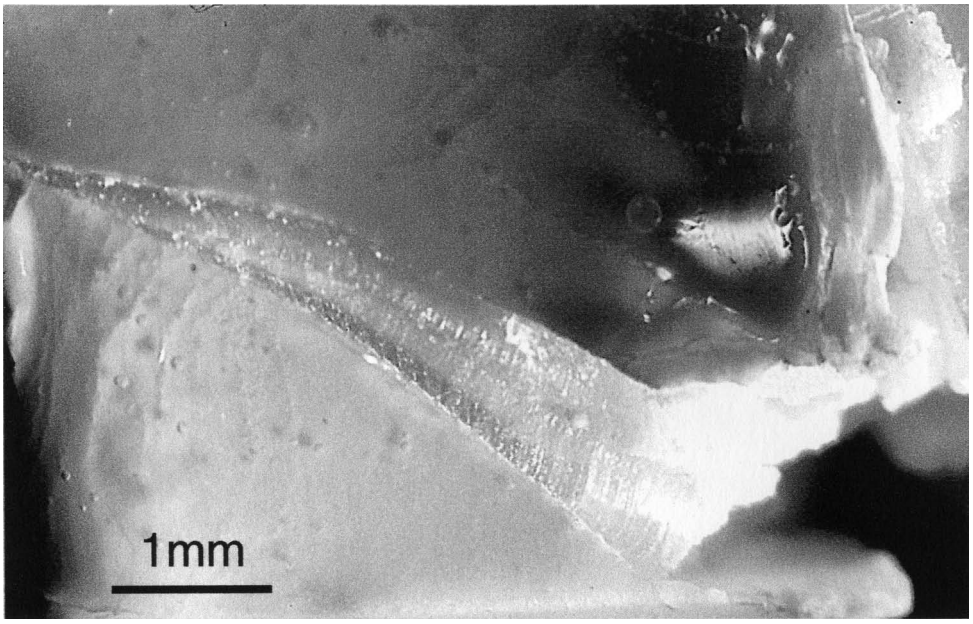

(f)

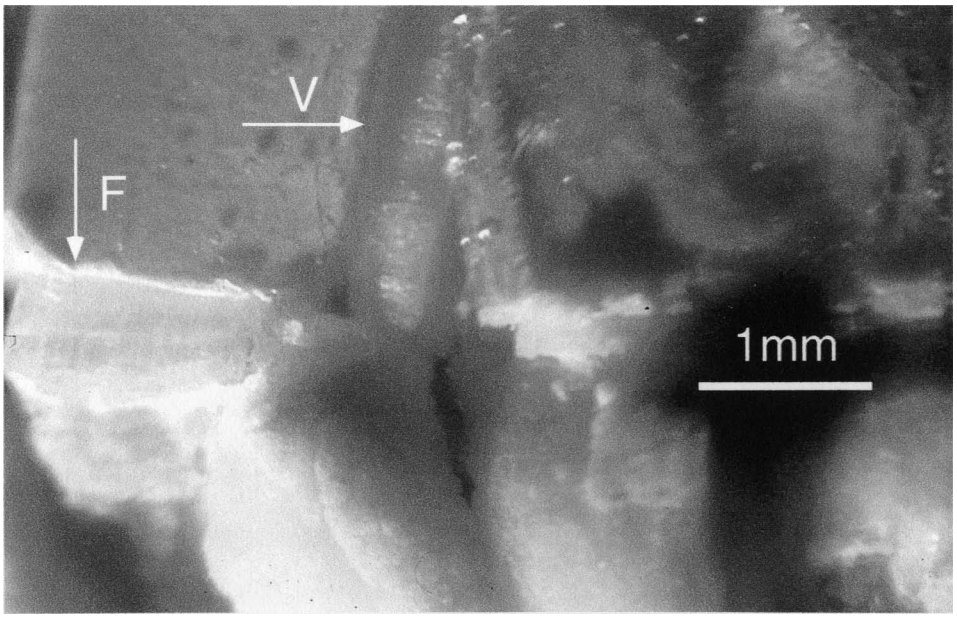

Fig. 4.9 Growth of fibers of N_aNO_3 at 'wrong' places in dead-weight experiments. (**a**) Plan view of the sample of experiment *DW-17* (dead-weight removed) showing thin sheets of fibers growing out of the edges of the crack between the upper and lower blocks due to the heavy dead-weight loading (7890 grams). Photograph taken at the same time as Fig. 4.6a. (**b**) Plan view of the sample of experiment *DW-18* (dead-weight removed) showing a new vein of fibers forced open by fiber growth in the right side of the upper epoxy-coated ceramic block due to the dead-weight loading (4000 grams). Also visible are some thin sheets of fibers grown out of the crack between the upper and lower blocks. Photograph taken at the same time as Fig. 4.6b. (**c**) Photograph of a thin sheet of fibers broken off the sample of *DW-17* showing fine texture and curved shape of the fibers. At least one type I transverse discontinuity and numerous type II transverse features are visible across the fibers.

(a)

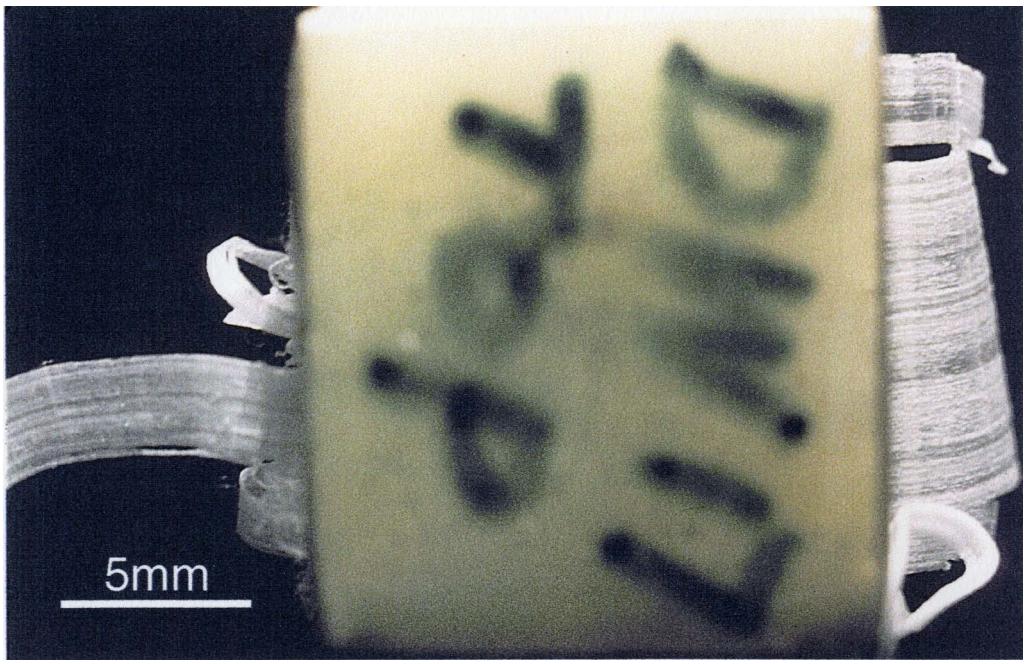

(b)

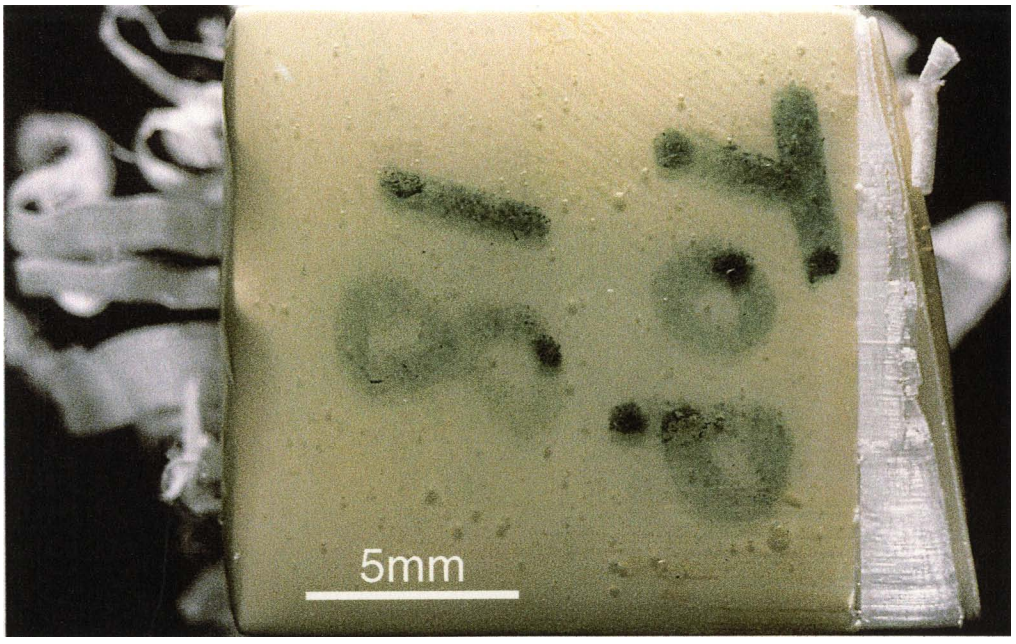

(c)

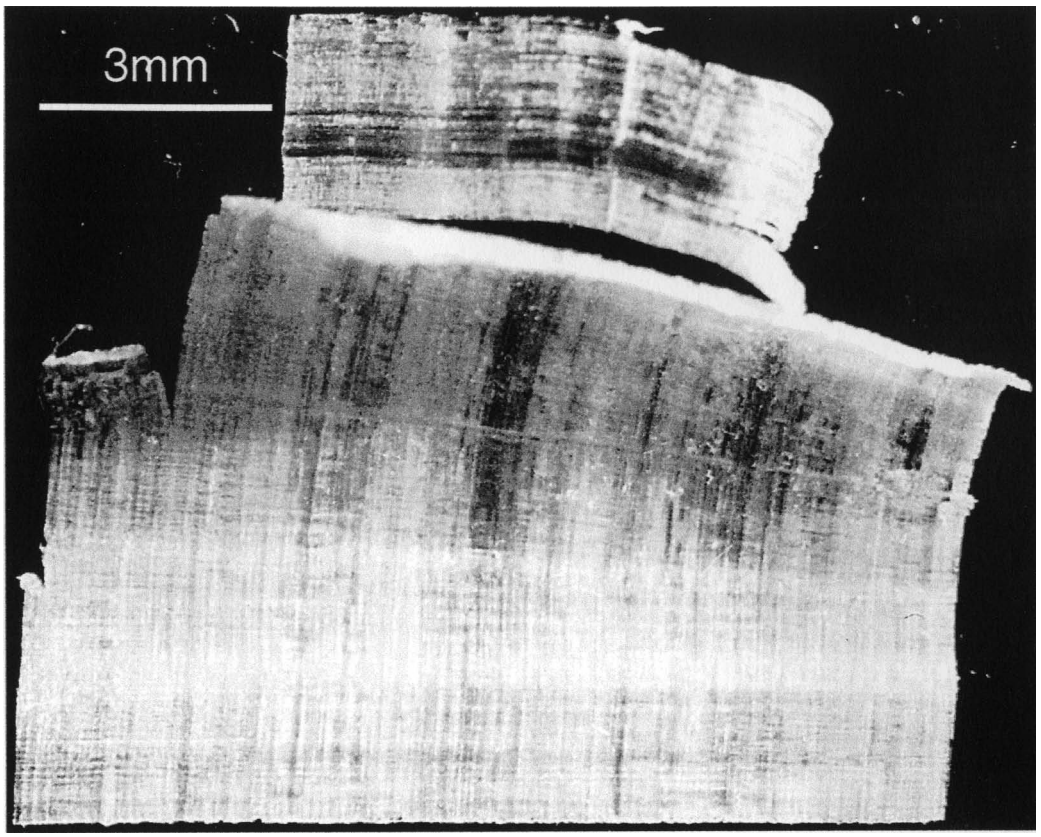

(a)

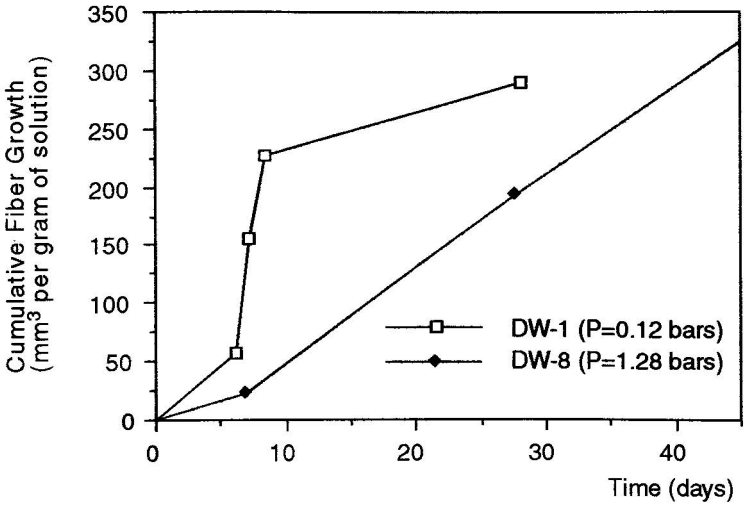

(b)

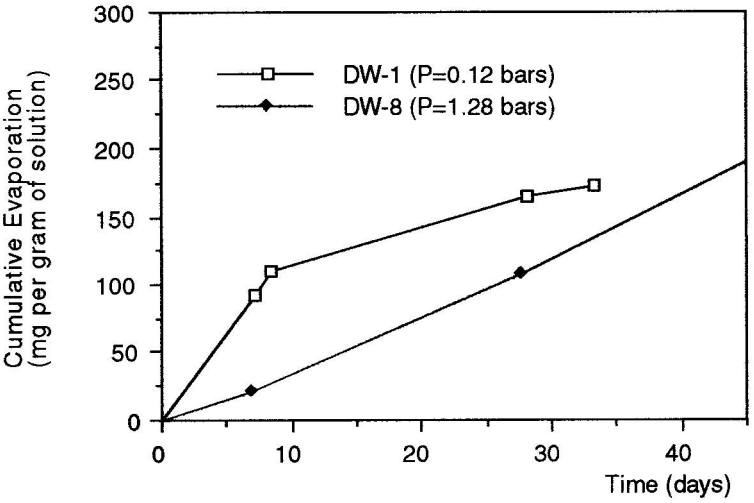

Fig. 4.10 Diagrams comparing the cumulative growth and evaporation as a function of time in two different dead-weight experiments with different loading pressures. (**a**) Diagram comparing the cumulative amount of vein growth as a function of time in experiments *DW-1* and *DW-8* (loading pressures shown). The cumulative growth is measured in terms of the volume of fibers (in mm^3) normalized against the total amount of solution (in grams) initially contained in the sample with an error of about ±10. (**b**) Diagram comparing the cumulative amount of loss of water by evaporation as a function of time in the same two experiments. The cumulative evaporation is measured in terms of the total amount of water lost at the time of observation normalized against the total amount of solution (in grams) initially contained in the sample with an error of about ±2. See text for details.

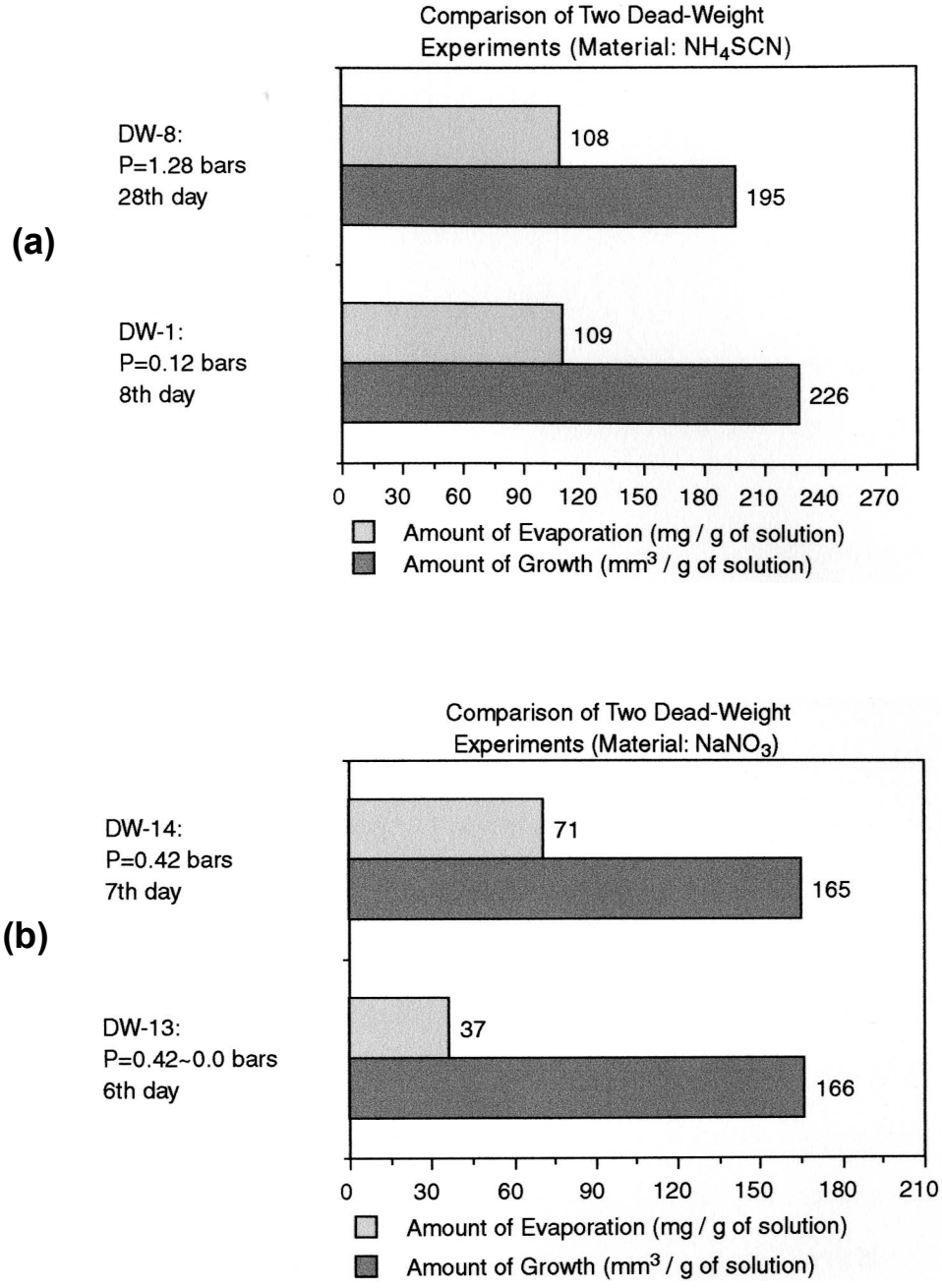

Fig. 4.11 Diagrams comparing the relative amounts of growth and evaporation in different dead-weight experiments with different loading pressures. (**a**) Diagram showing different cumulative amounts of growth in experiments *DW-1* and *DW-8* at different times when their cumulative evaporations were approximately the same. (**b**) Diagram showing different cumulative amounts of evaporation in experiments *DW-13* and *DW-14* at different times when their cumulative amounts of growth were approximately the same. The cumulative amount of growth and cumulative amount of evaporation are expressed in the same units as in Fig. 4.10. The error of measurement for the amount of evaporation is about ±2, while that for the amount of growth is about ±10.

Fig. 4.12 Diagrams showing the detailed loading, evaporation and growth histories of a two-sample dead-weight experiment *DW-11&12*. (**a**) shows the dead-weight loading pressure changes and temperature variation as a function of time in the experiment. (**b**) shows the cumulative evaporations of the two samples as a function of time, expressed in terms of milligrams of the cumulative loss of water per gram of solvent initially contained in the samples. The error of measurement is about ±5. (**c**) shows the average widths of the veins in the two samples at five successive times of observation. The error of measurement is about ±50μm. Arrows on the horizontal axis indicate the five different times the veins were photographed (corresponding pictures of DW-11 and DW-12 shown in Figs. 4.13 and 4.14, respectively). See text for details.

(a)

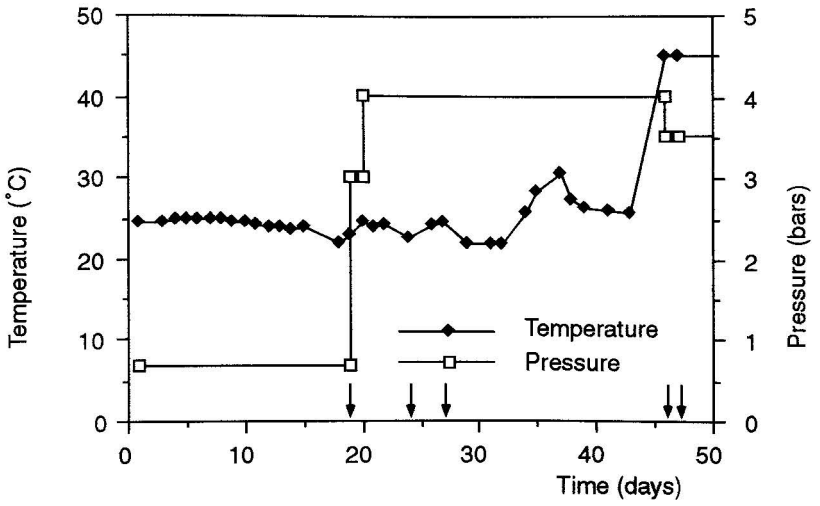
Temperature (°C)
Pressure (bars)
Time (days)
Temperature
Pressure

(b)

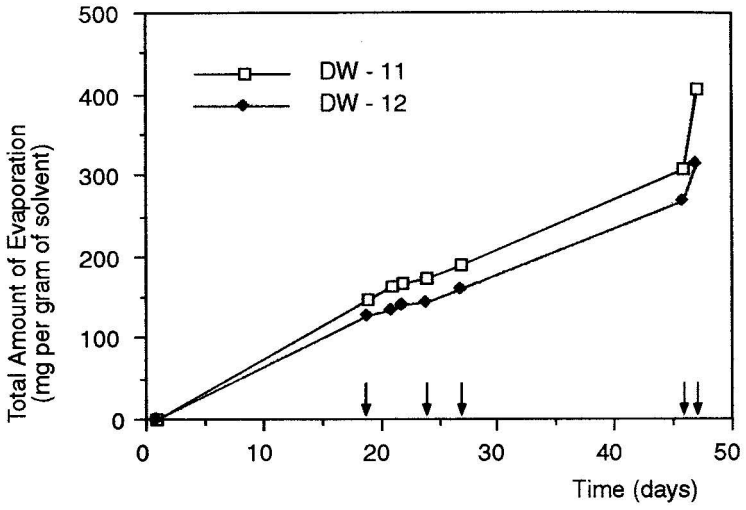
Total Amount of Evaporation
(mg per gram of solvent)
Time (days)
DW - 11
DW - 12

(c)

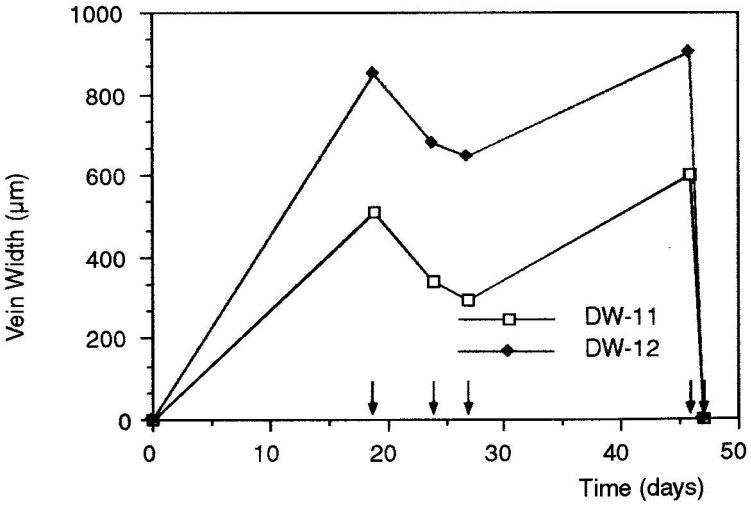
Vein Width (µm)
Time (days)
DW-11
DW-12

Fig. 4.13 Photographs showing history of opening and closing of the vein of fibers of NH_4SCN in sample *DW-11* under changing dead-weight loading pressure and temperature conditions in experiment *DW-11&12*. Numbers in the upper left corner of each picture represent the times at which the photographs were taken and correspond to the time positions indicated by arrows in Fig. 4.12. (**a**) View of the vein grown under a dead-weight loading pressure of 0.7 bars in the first loading stage. Photograph taken immediately before the pressure was increased to 3 bars and then to 4 bars at day 20. (**b**) Same view of the vein shrinked due to the increased loading pressure. Fibers still show their vertical orientations and no signs of any significant flattening or collapsing can be seen in the vein. (**c**) Same view of the vein 3 days later. Unlike other views of the vein, the vein at this site does not show significant shrinkage at this stage. Note the bay-like indentations along the contact between the vein and the upper wall. (**d**) Same view of the vein 19 days later. The vein thickness has increased significantly under the same loading pressure conditions. After this photograph was taken, the temperature was increased from about 25° to 45°. (**e**) Same view of the vein the next day. The vein has completely closed due to dissolution of the fibers under the increased temperature and the large pressure conditions.

(a)

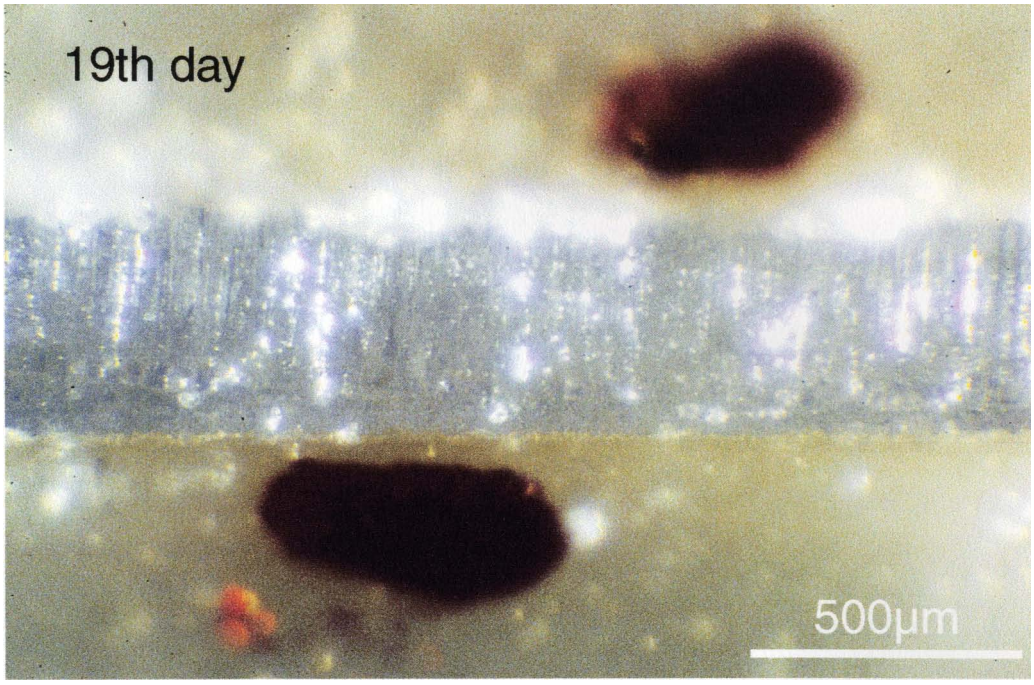

(b)

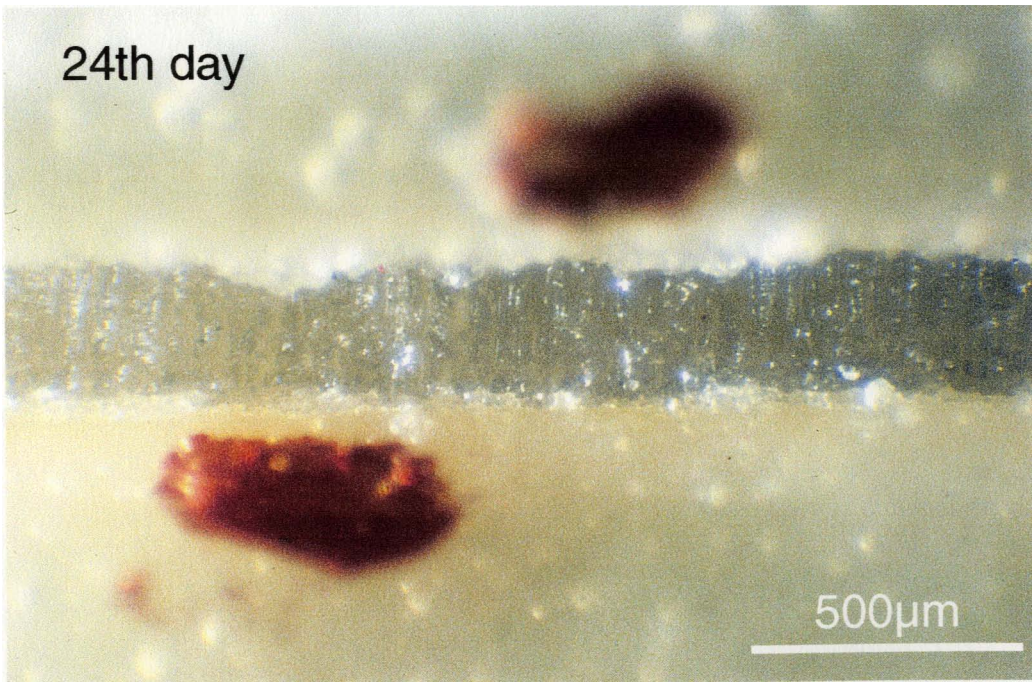

(c)

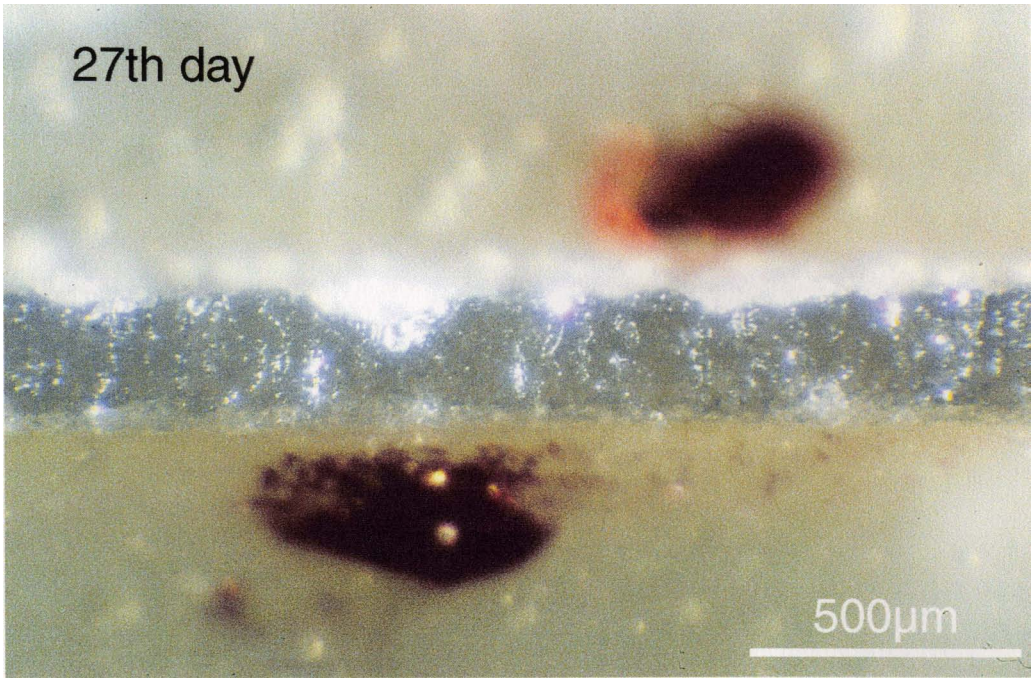

(d)

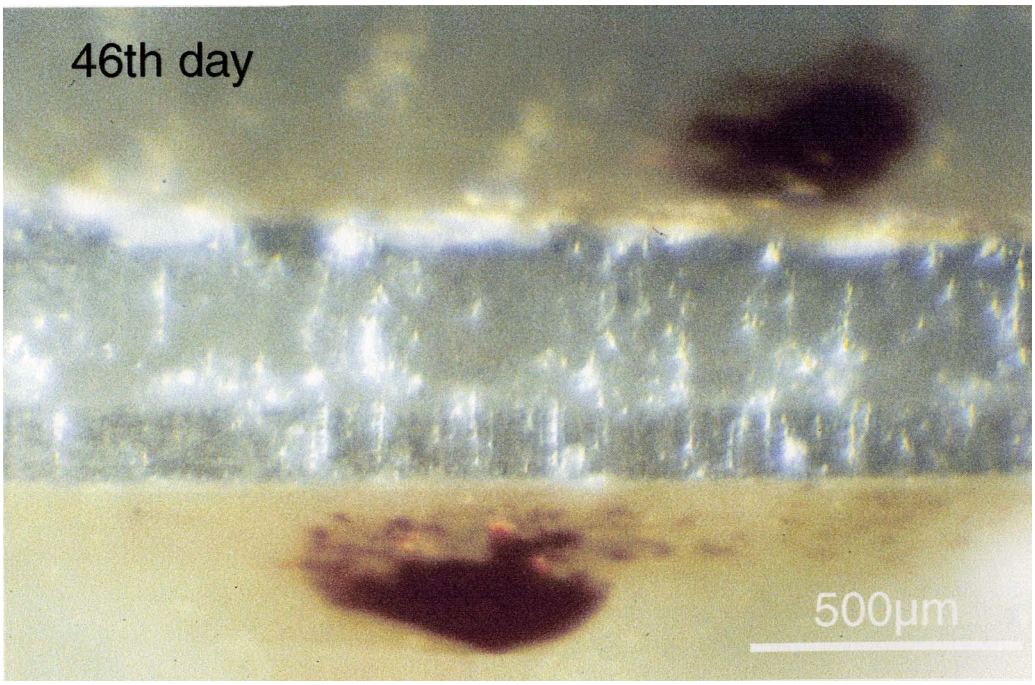

(e)

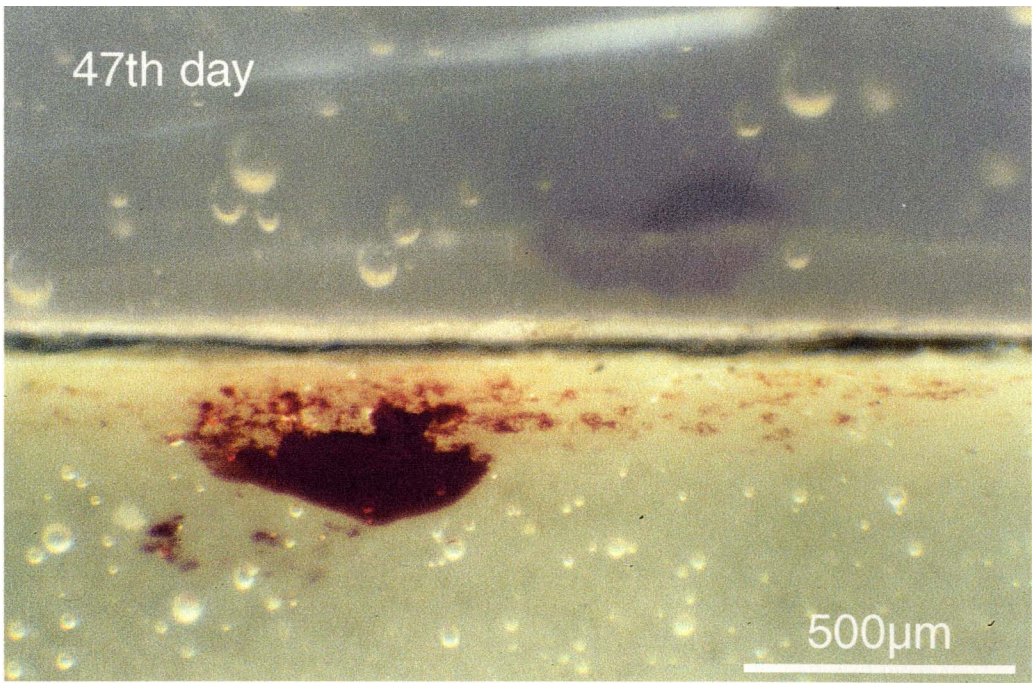

Fig. 4.14 Photographs showing history of opening and closing of the vein of fibers of *NH_4SCN* in sample *DW-12* under changing loading pressure and temperature conditions in dead-weight experiment *DW-11&12*. Numbers in the upper left corner of each picture represent the times at which the photographs were taken and correspond to the time positions indicated by arrows in Fig. 4.12. (**a**) View of the vein grown under a loading pressure of 0.7 bars in the first stage. Photograph taken immediately before the pressure was increased to 3 bars and then to 4 bars at day 20. (**b**) Same view of the vein shrinked due to the increased pressure. Fibers do not show signs of any significant flattening or collapsing except for some bay-like indentations along the contact between the vein and the upper wall. (**c**) Same view of the vein 3 days later. It does not show much change in thickness as seen in this view of the vein. (**d**) Same view of the vein 19 days later. As seen in this veiw, the vein does not show much change in total thickness, but it clearly shows fresh fibers between a greatly narrowed central old vein and the upper and lower walls, grown during the later part of the last 19-day period under the same pressure conditions that previously caused dissolution. After this photograph was taken, the temperature was increased from about 25° to 45° . (**e**) Same view of the vein on the next day. The vein has completely closed due to dissolution of the fibers under the increased temperature and the large pressure conditions. Note there are still some free crystals on the edges of the vein.

(a)

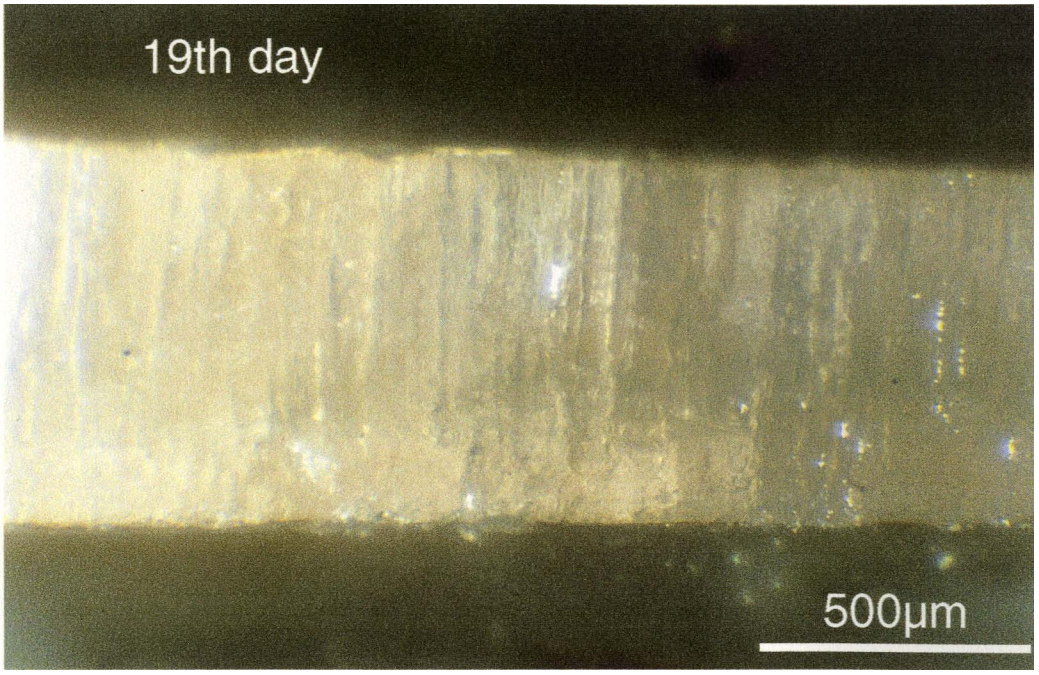

(b)

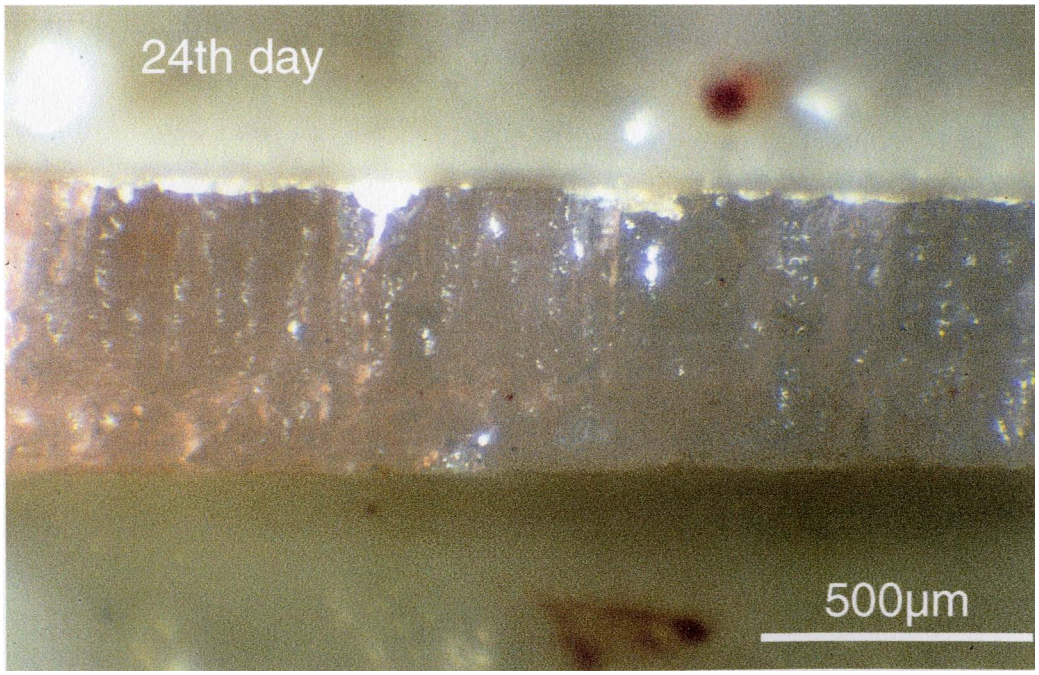

(c)

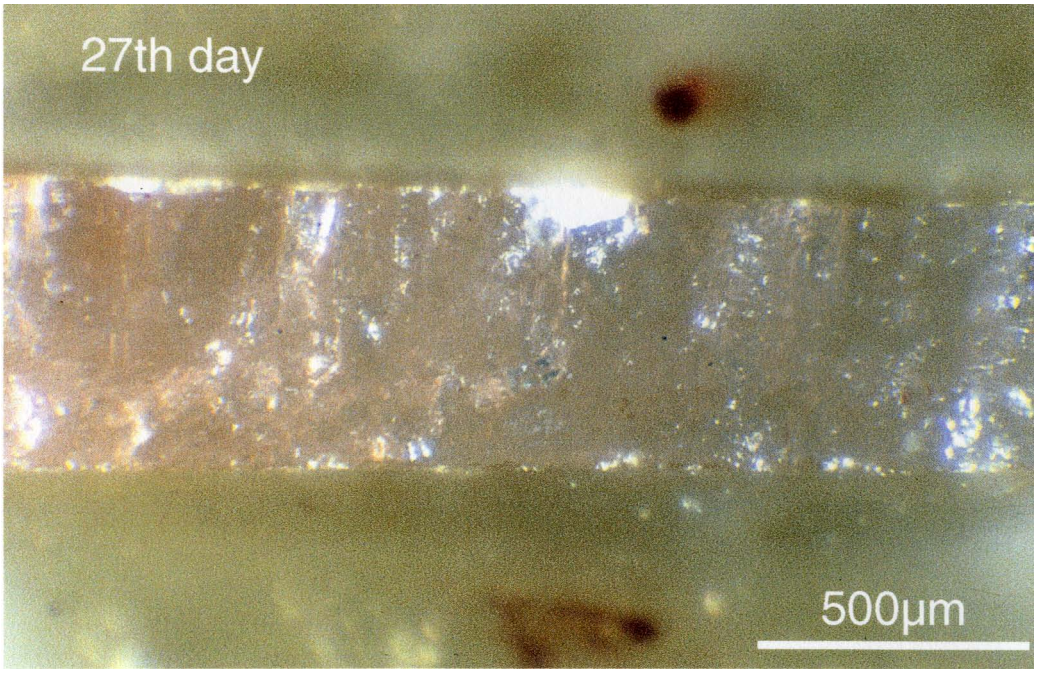

(d)

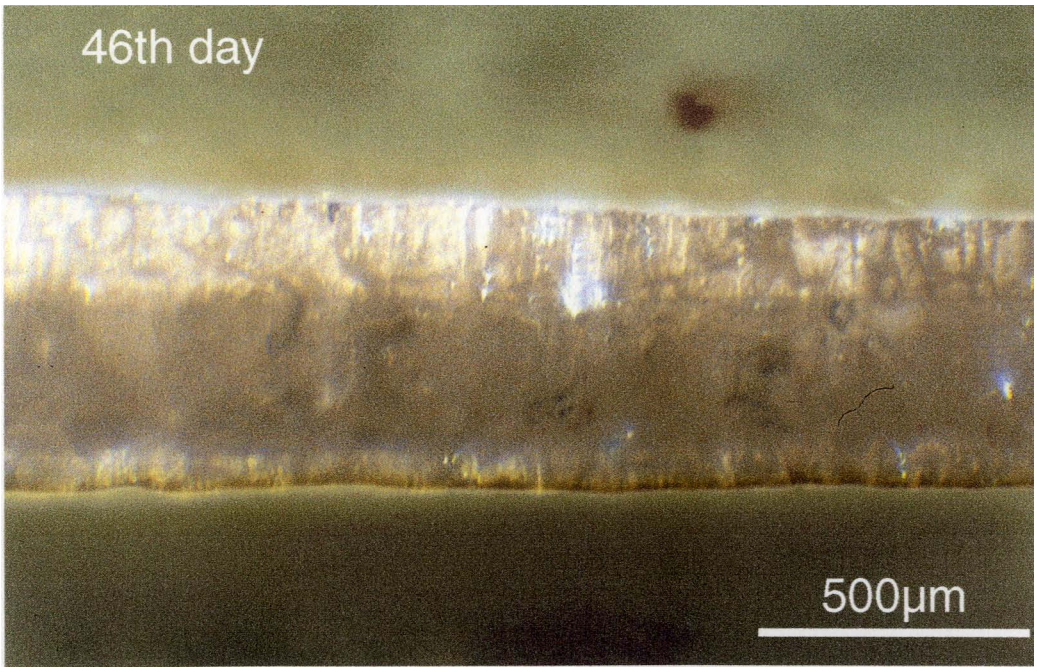

(e)

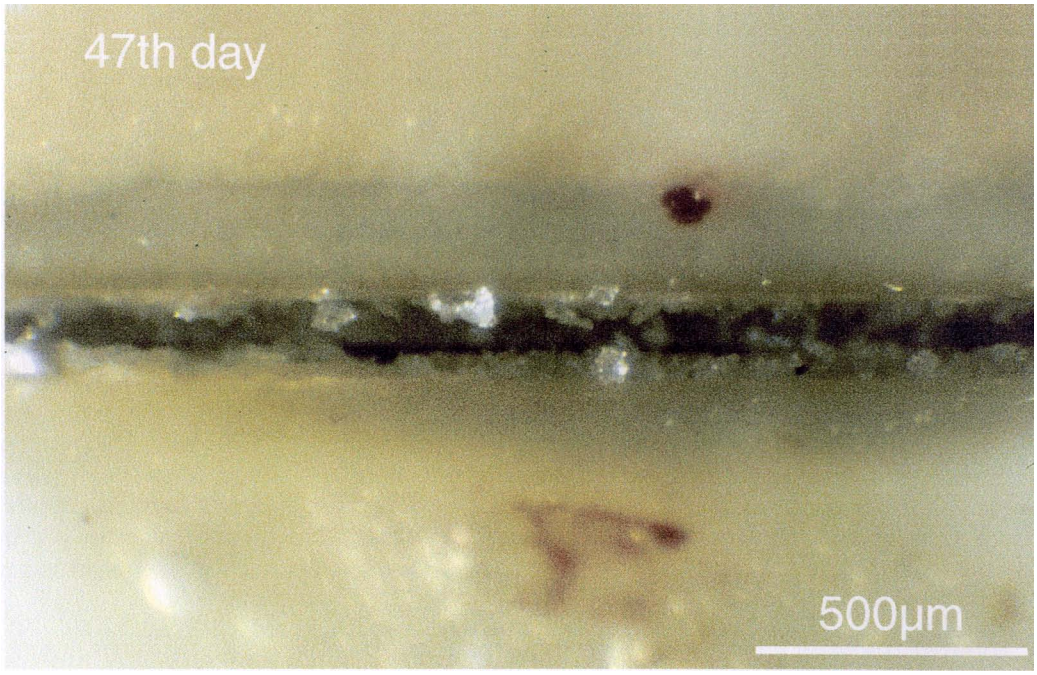

Fig. 4.15 Photographs showing history of opening and closing of the vein in sample *DW-12* seen on another side of the sample (side B). Numbers in the upper part of each picture represent the times at which the photographs were taken and correspond to the first 4 time positions indicated by arrows in Fig. 4.12. (**a**) View of the vein at this site at the first time of observation. After this photograph was taken, the loading pressure was first increased to 3 bars and then to 4 bars on the next day. (**b**) Same view of the vein 5 days later. It has been greatly shrinked due to the increased pressure. No signs of significant flattening or collapsing are visible in the fibers. (**c**) Same view of the vein 3 more days later. The vein width has further decreased slightly at this site. (**d**) Same view of the vein 19 days later, showing much renewed dilation under the same pressure conditions that caused previous dissolution. The vein also clearly shows a further shrinked older central vein followed by new growth of fresh fibers at the edges of the upper and lower walls, indicating that dissolution must have continued well into this stage of experiment.

(a)

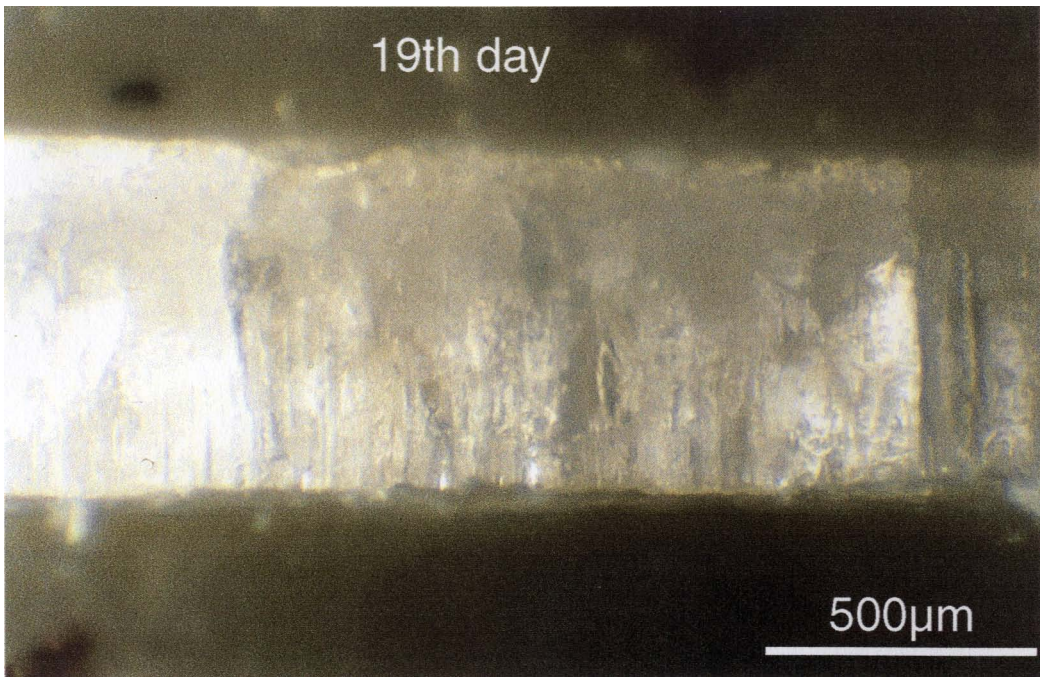

(b)

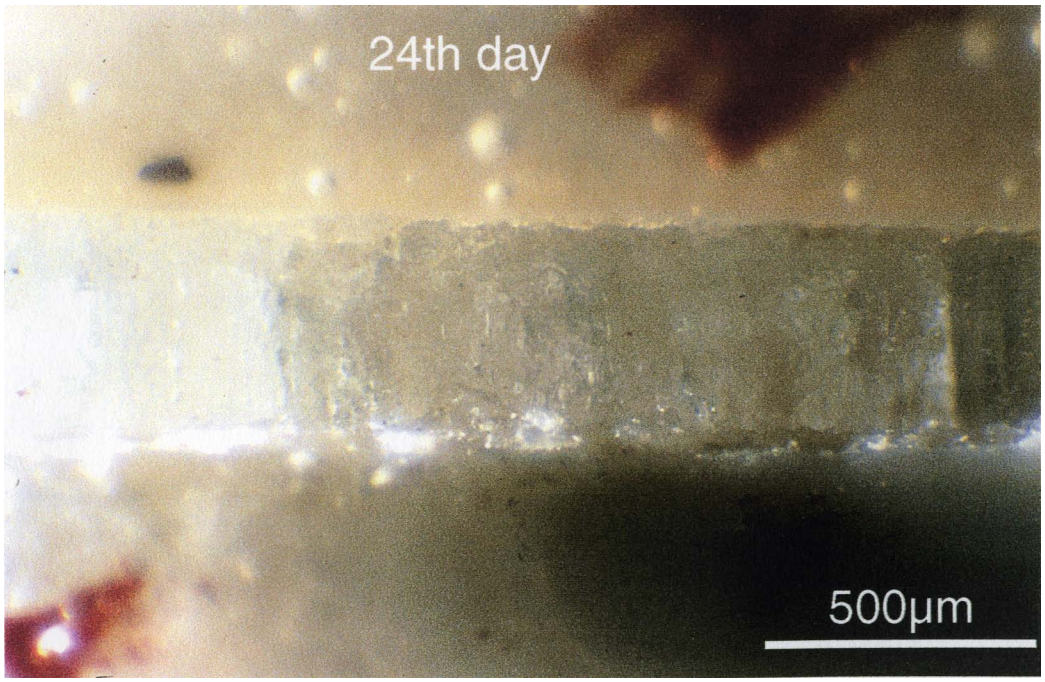

(c)

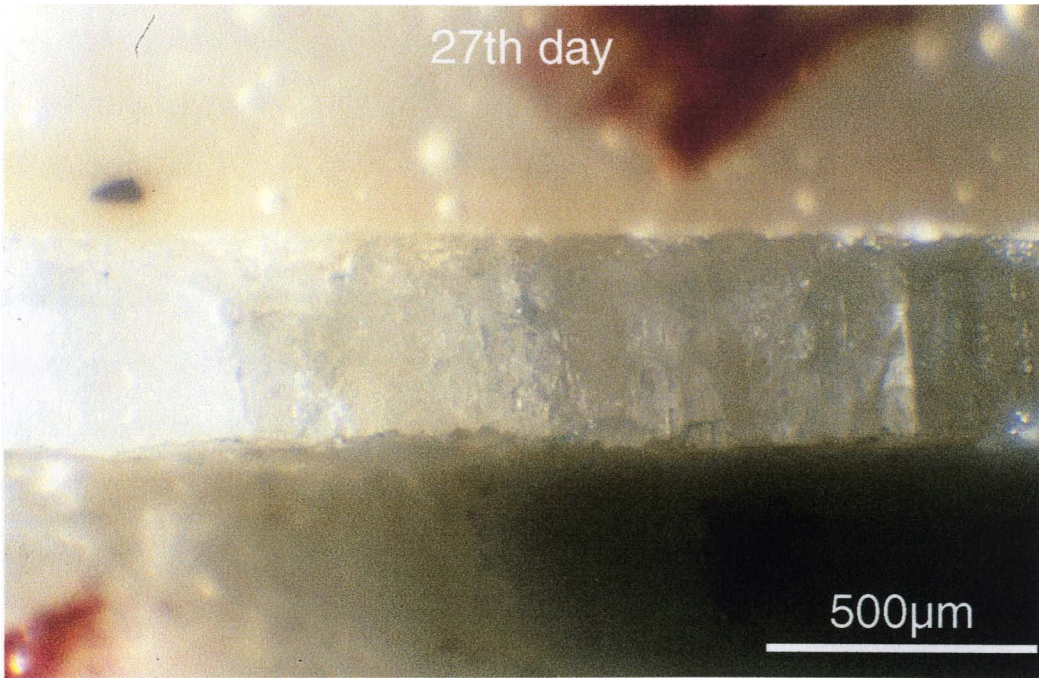

(d)

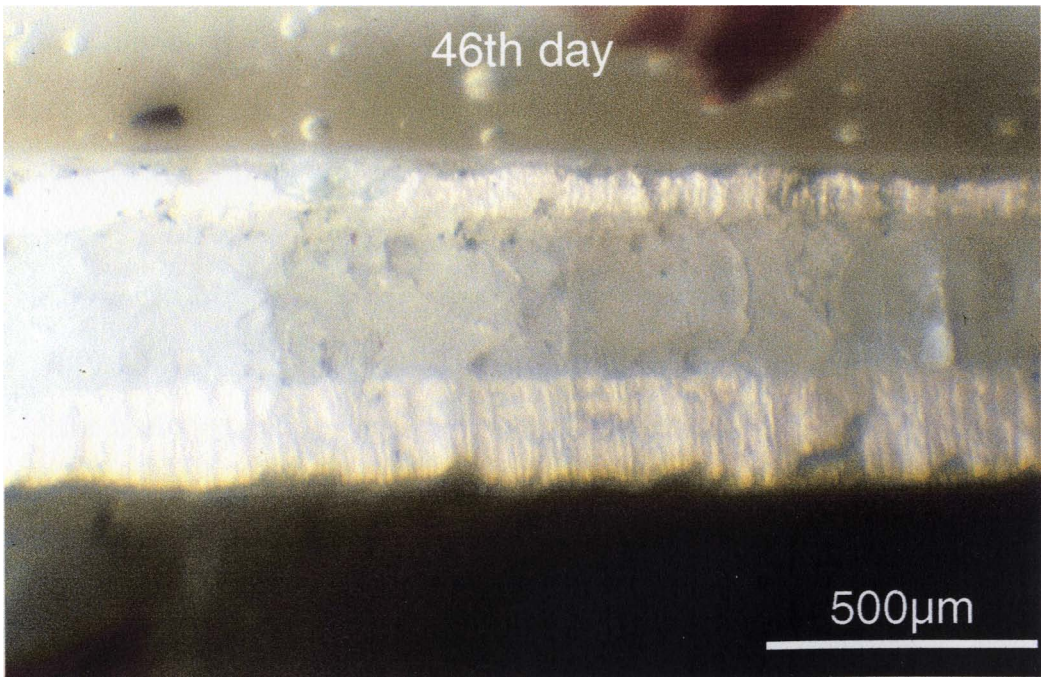

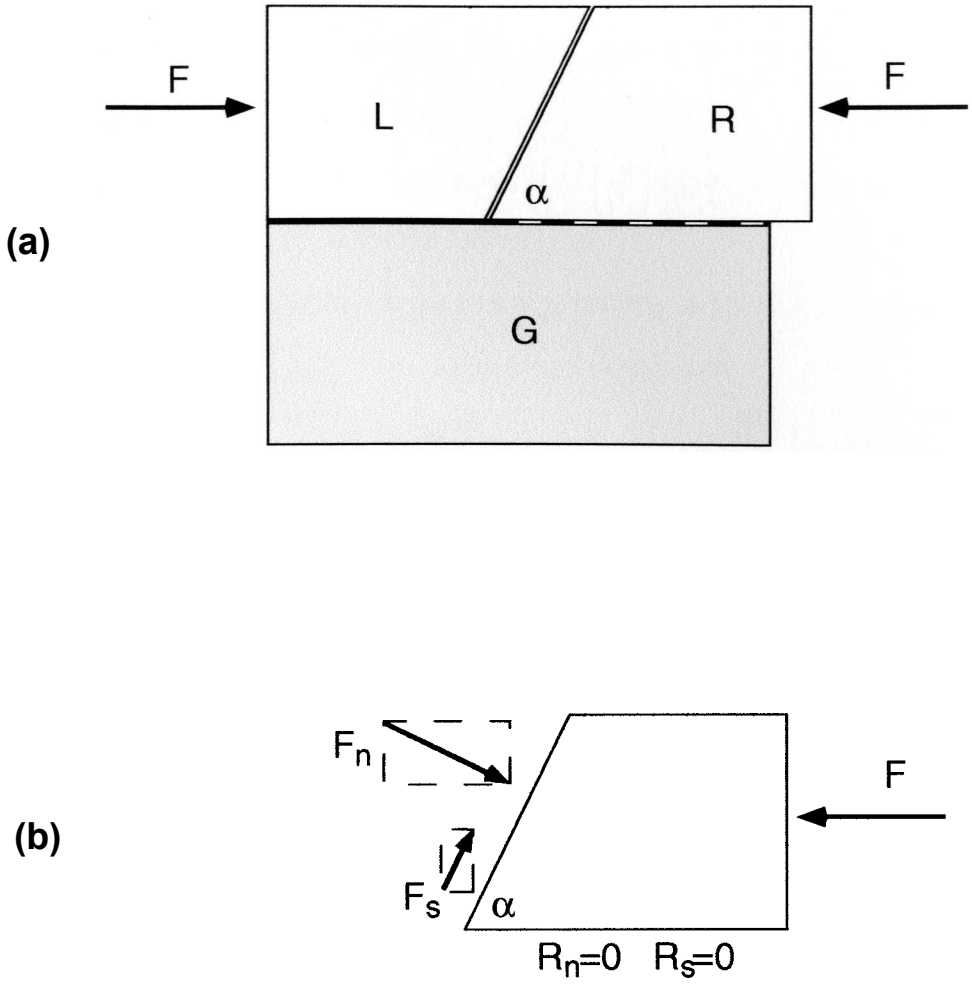

Fig. 4.16 Schematic diagrams showing forces exerted on the ceramic blocks at the beginning of an oblique rubber-band loading experiment in which α is larger than the angle of repose of the crack surface. (**a**) Plan view of the set-up (refer to Fig. 4.2). The left block (L) is glued to the guide (G) while the right block (R) is free to slide on the guide. A compressive loading force (F) is imposed on the blocks by means of a rubber band. (**b**) Free-body diagram of the right block at the beginning of experiment (gravity is ignored). R_n and R_s are the normal and shear forces of reaction on the contact surface of the right block with the guide, while F_n and F_s are the normal and shear forces exerted to the right block by the left block.

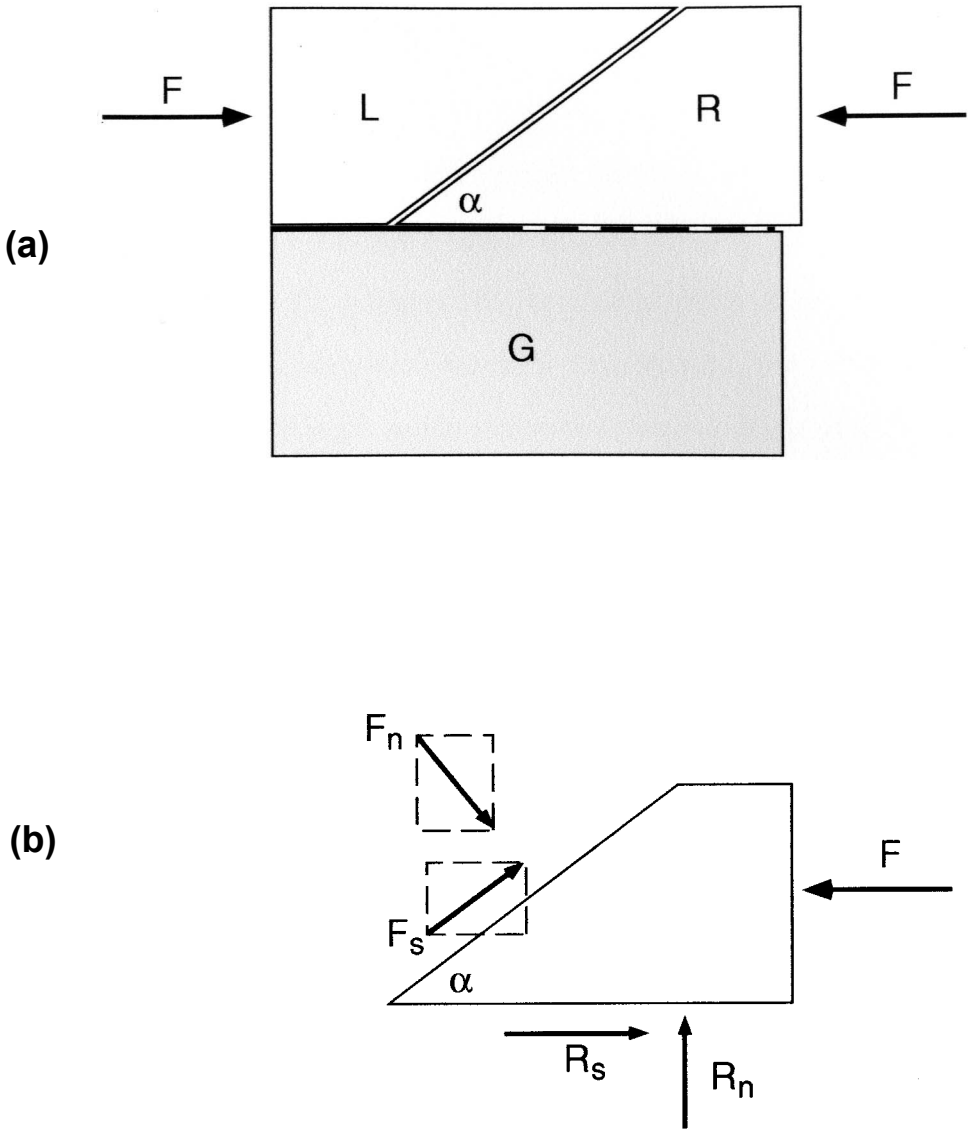

Fig. 4.17 Schematic diagrams showing forces exerted on the ceramic blocks at the beginning of a highly oblique rubber-band loading experiment (α is smaller than the angle of repose of the crack surface). (**a**) Plan view of the set-up (refer to Fig. 4.2). The left block (L) is glued to the guide (G) while the right block (R) is free to slide on the guide. A compressive force (F) is imposed on the blocks by means of a rubber band. (**b**) Free-body diagram of the right block at the beginning of experiment (gravity is ignored). R_n and R_s are the normal and shear forces of reaction on the contact surface of the right block with the guide, while F_n and F_s are the normal and shear forces exerted to the right block by the left block.

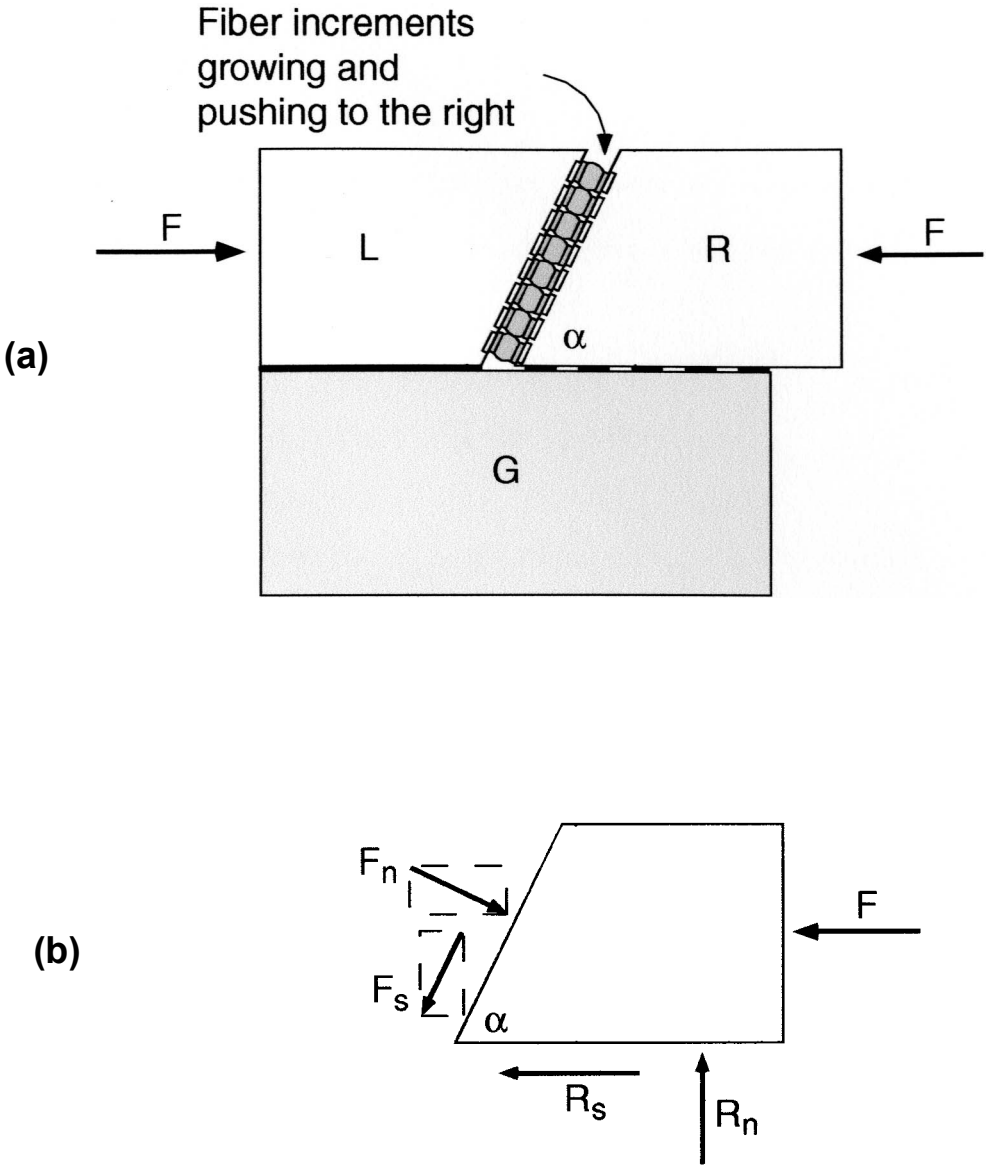

Fig. 4.18 Schematic diagrams showing forces exerted on the ceramic blocks *during* a rubber-band loading experiment. (a) Plan view of the set-up (refer to Fig. 4.2). The left block (L) is glued to the guide (G) while the right block (R) is free to slide on the guide. A compressive force (F) is imposed on the blocks by means of a rubber band. Taber growth tends to push the right block to the right. (b) Free-body diagram of the right block during fiber growth. R_n and R_s are the normal and shear forces of reaction on the contact surface of the right block with the guide, while F_n and F_s are the normal and shear forces exerted to the right block by the growing fibers. Note the directions of R_s and F_s are opposite to those in Figs. 4.16 & 4.17.

Fig. 4.19 Growth of a vein of fibers of NH_4SCN in a rubber-band loading experiment (*DW-3*) with a moderate angle of obliquity (α=55.6°) of the crack with respect to the loading, seen on the normal face of the sample. The first 3 photographs are aligned such that the guide (out of the view, on the top side of the picture) runs parallel to the horizontal, and the left block (glued on the guide) is fixed in position with respect to the picture while the right block is displaced by fiber growth (refer to Figs. 4.2 & 4.18). The date and time of photography is shown at the top of each photograph.
(**a**) Initial crack between the blocks at the beginning of experiment. Black spots alongside of the crack are metal power particles embedded into the wet epoxy-coating during the sample preparation process to serve as markers for monitoring relative displacements between the blocks.
(**b**) Opened vein formed by fibers pushing the right block to the right during the first 25 days. Fibers are seen to be roughly parallel to the (horizontal) guide.
(**c**) Greatly widened vein another 27 days later. Fibers are syntaxially curved with younger fibers lying at increasingly high angles to the walls. Between the two asymmetrically developed vein halves is a pronounced discontinuity along which the right block could be easily detached from the left block.
(**d**) Detached left half of the vein showing the syntaxial pattern of curved fibers.
(**e**) Enlarged view of part of the vein shown in (b) showing the overall guide-parallel fibers are actually syntaxially curved.
(**f**) Enlarged view of part of the half vein shown in (d).

(a)

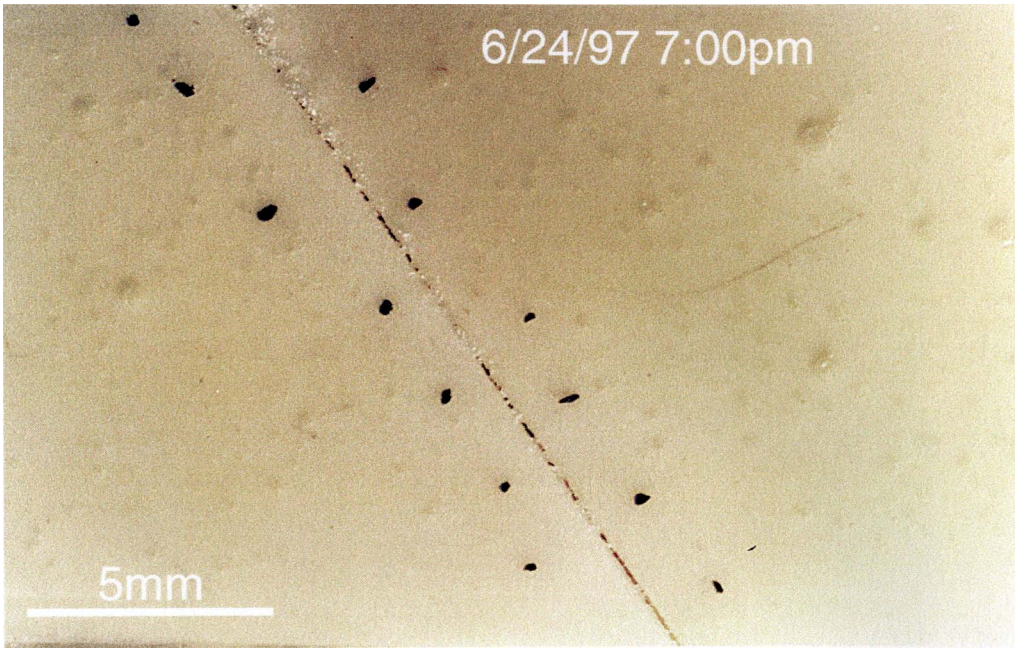

(b)

(c)

(d)

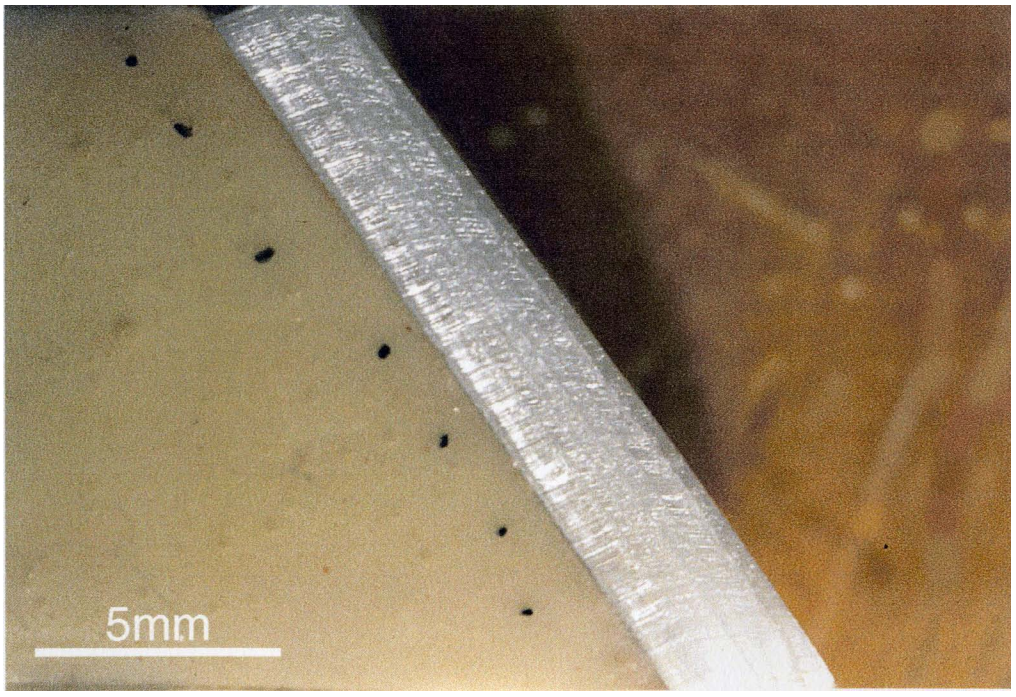

(e)

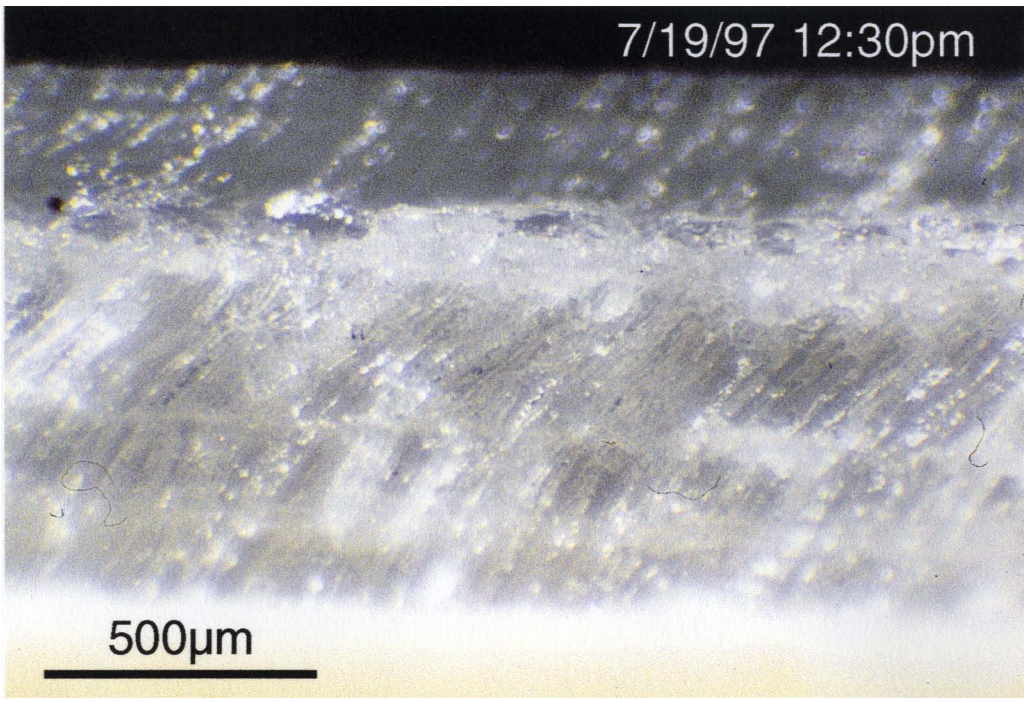

(f)

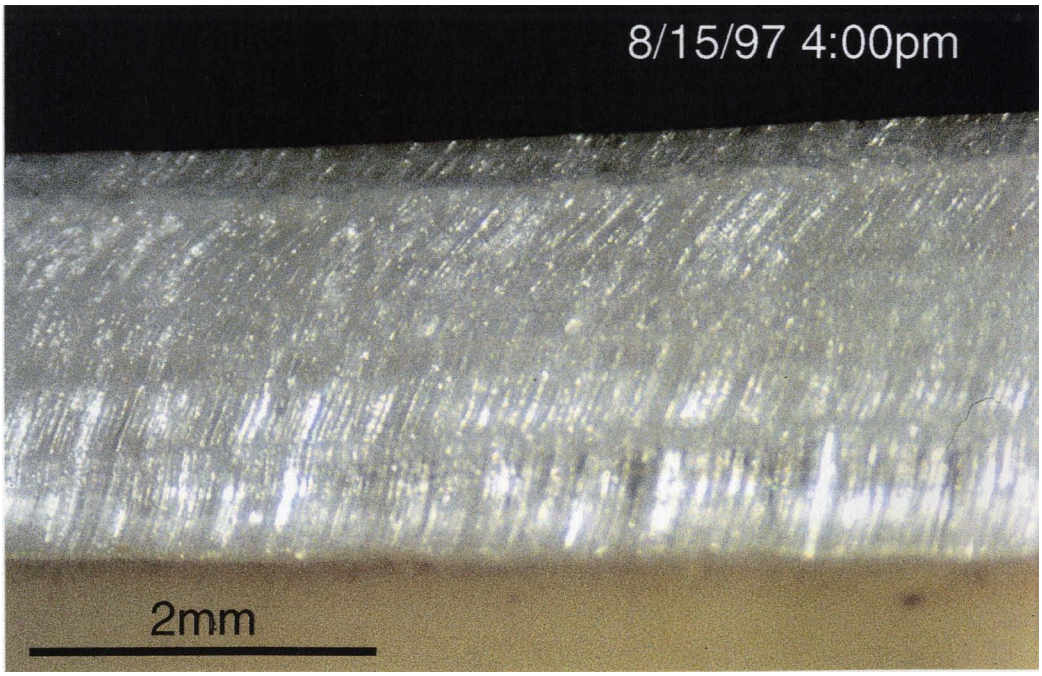

Fig. 4.20 Vein growth in the same experiment as in Fig. 4.19, seen on the other face of the sample. The first 2 photographs are aligned such that the guide (out of the view, on the top side of the picture) runs parallel to the horizontal, and the right block (glued on the guide) is fixed in position with respect to the picture while the left block is displaced by fiber growth (refer to Figs. 4.2 & 4.18). The date and time of photography is shown at the top of each photograph.
(**a**) Initial crack between the blocks at the beginning of experiment.
(**b**) Opened vein formed by fibers pushing the left block to the left during the first 25 days. Fibers grown from the left block (the free block) are better developed than fibers from the right block and assume a markedly different orientation from that of the (horizontal) guide.
(**c**) Enlarged view of part of the detached left half vein (grown from the free block) showing an overall syntaxial curvature pattern of fibers.

(a)

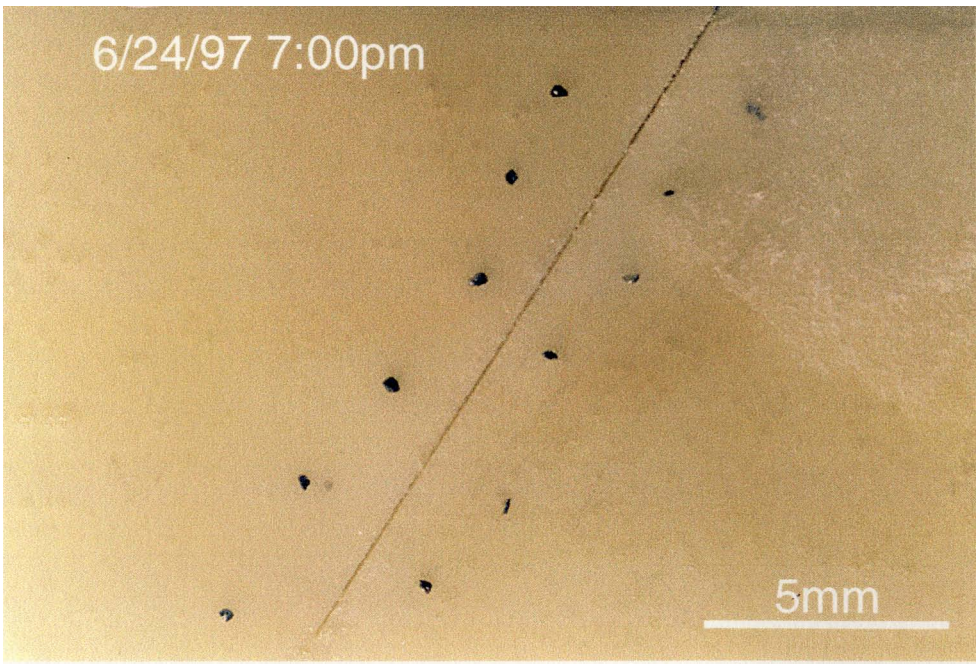

(b)

(c)

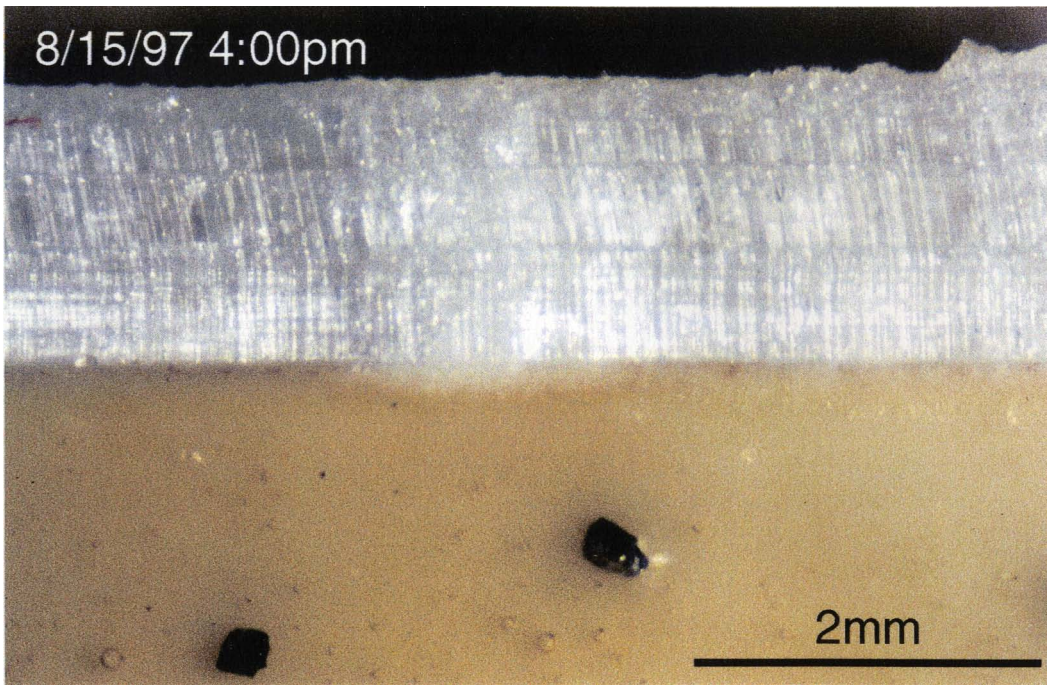

Fig. 4.21 Growth of a vein of fibers of NH_4SCN in a rubber-band loading experiment (*DW-7*) with a relative small degree of obliquity (α=64.5 °) of the crack with respect to the loading. The first 3 photographs are aligned such that the guide (out of the view, on the bottom side of the picture) runs parallel to the horizontal. The left block is the one epoxyed on the guide while the right block is the one intended to slide freely on the guide (refer to Figs. 4.2 & 4.18). The date and time of photography is shown at the top of each photograph.
(**a**) Initial crack between the blocks at the beginning of experiment. Black spots alongside of the crack are metal power particles embedded into the wet epoxy-coating during the sample preparation process to serve as markers for monitoring relative displacements between the blocks.
(**b**) Vein opened between the blocks by fibers growing and pushing the right block to the right along the guide during the first 12 days. Fibers are seen to be parallel to the (horizontal) guide.
(**c**) Further opening of the vein over the next 21 days. Fibers are still parallel to the (horizontal) guide, Red-colored lines show the orientation of the guide and were marked on the surface of the sample after photograph in (b) was taken.
(**d**) Enlarged view of the vein in (c) with the vein aligned parallel to the horizontal.
(**e**) & (**f**) Enlarged views of a particular site of the vein seen at the second and third stages of growth showing details of the straight, guide-parallel fibers in the vein.

(a)

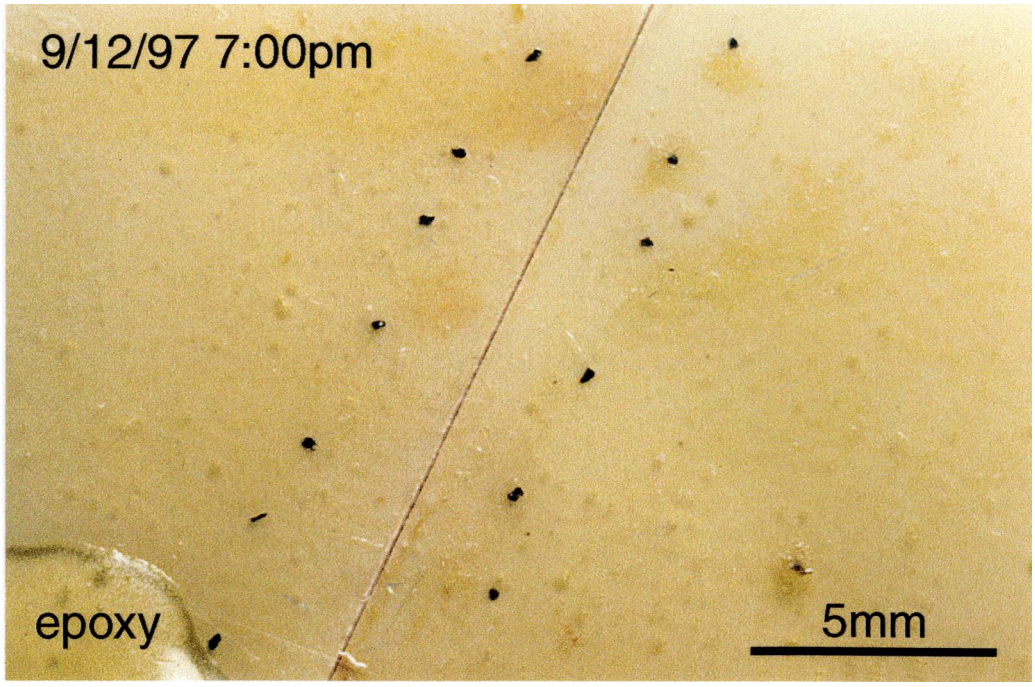

(b)

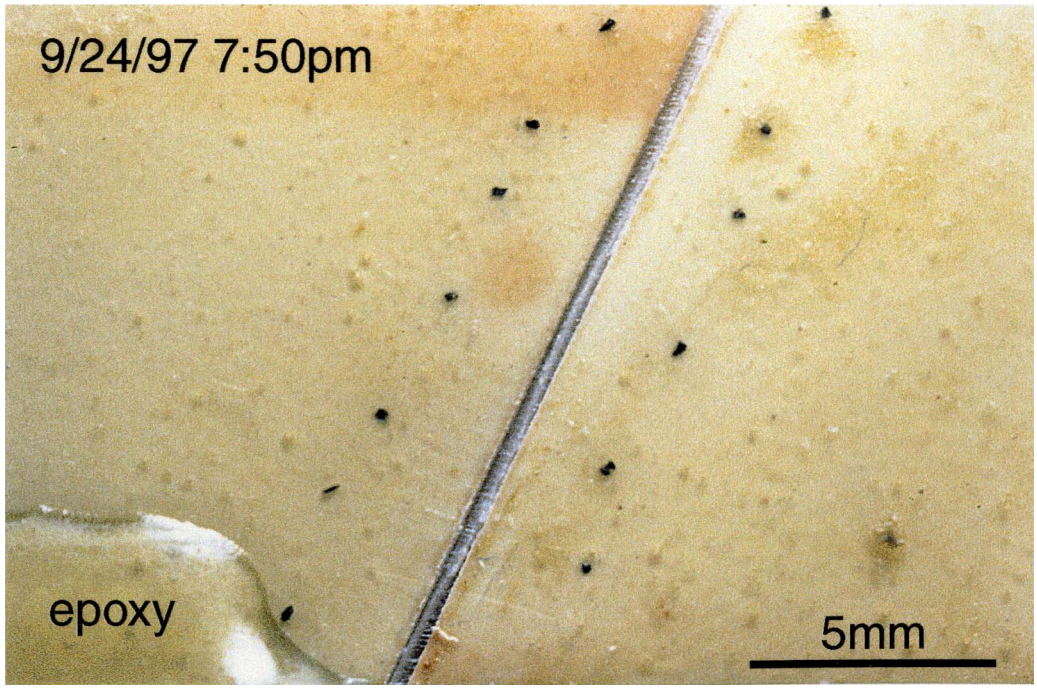

(c)

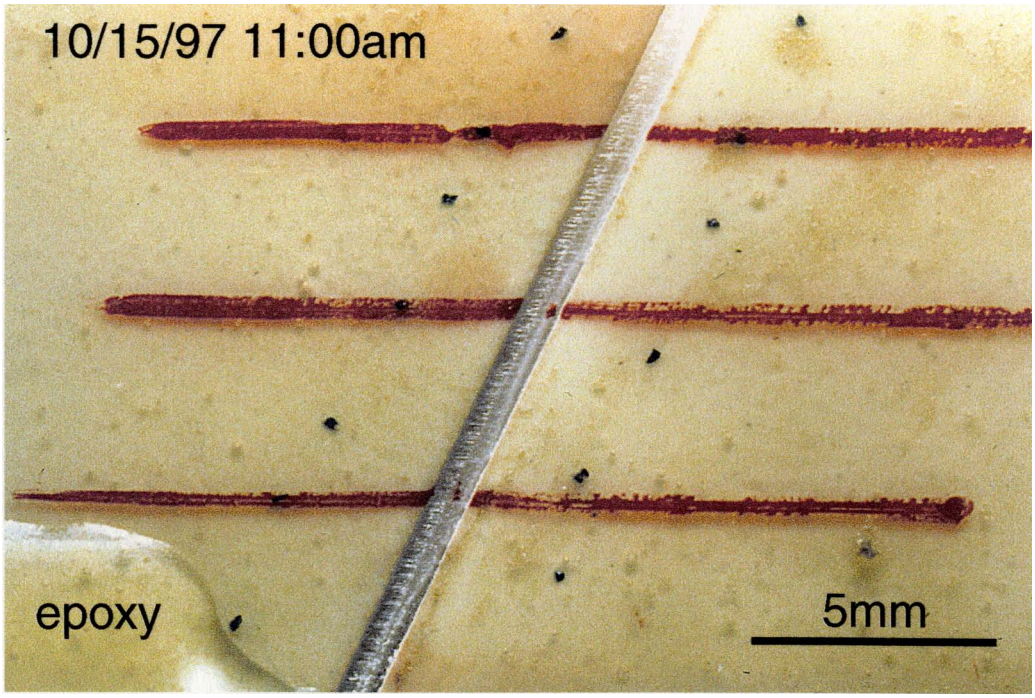

(d)

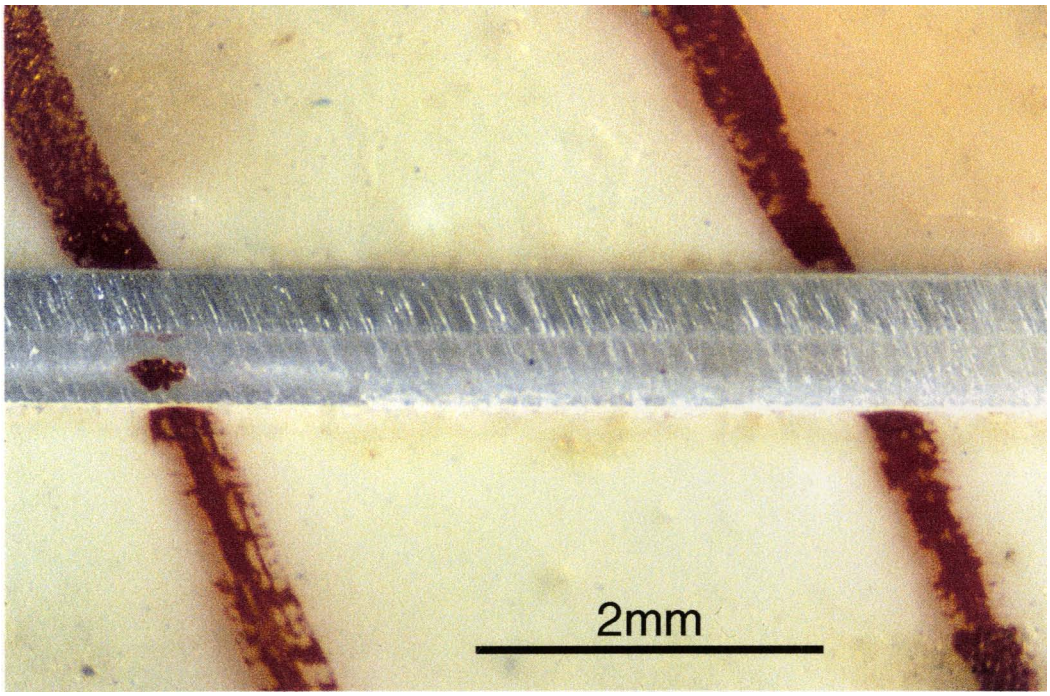

(e)

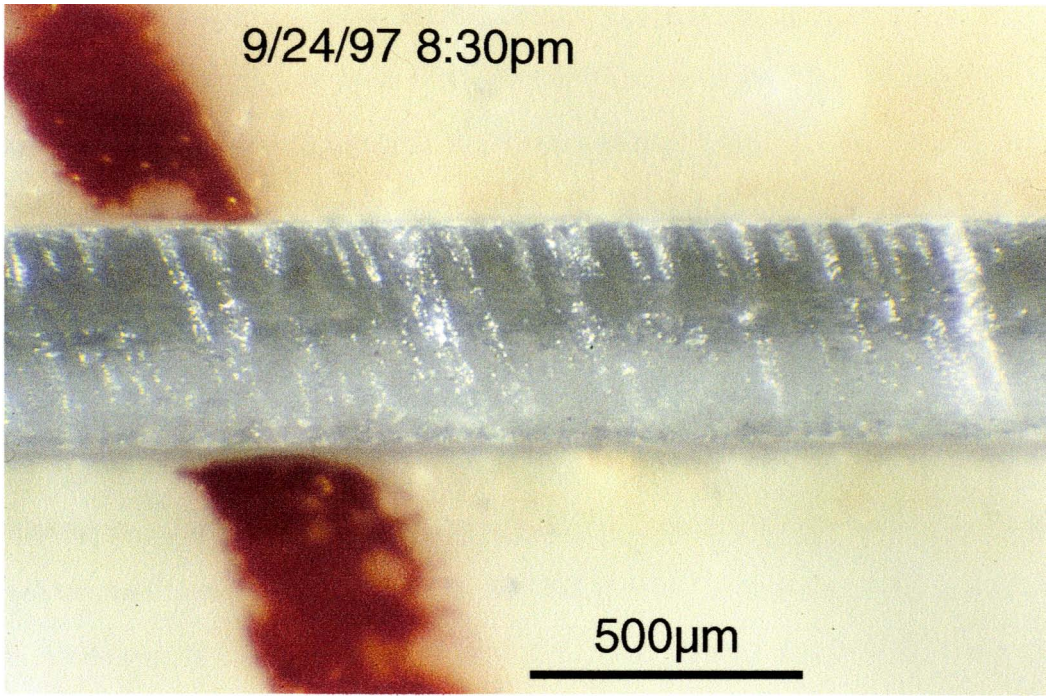

(f)

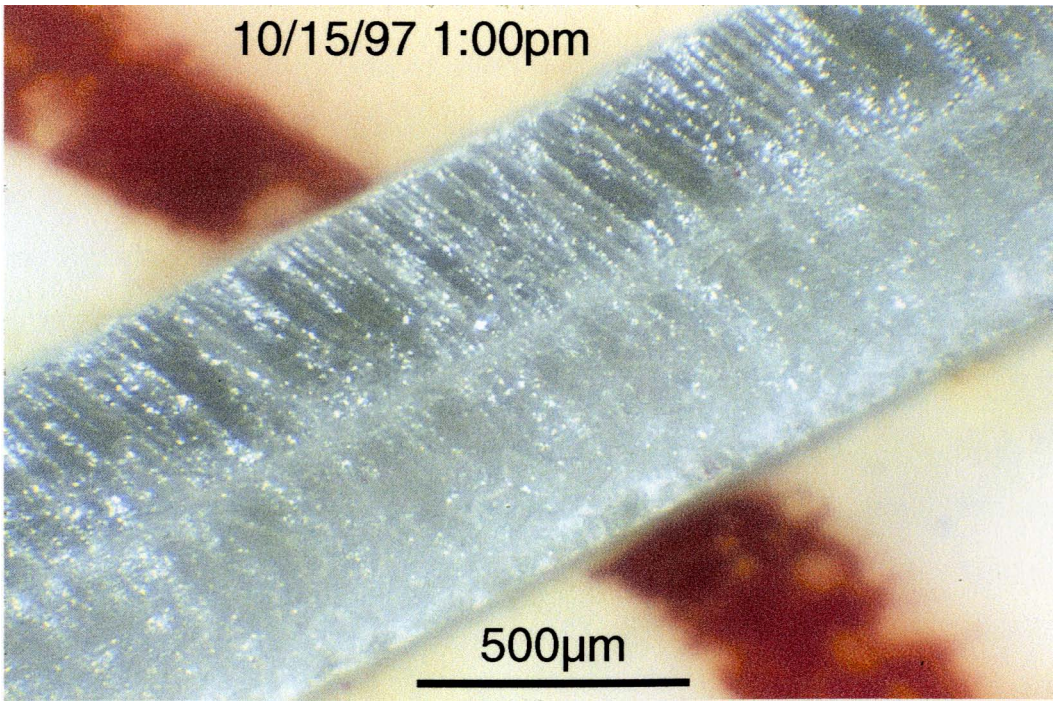

Fig. 4.22 Growth of a vein of fibers of NH_4SCN in a rubber-band loading experiment (*DW-6*) with a relative large degree of obliquity (α=32.2°) of the crack with respect to the loading. The first 4 photographs are aligned such that the guide (out of the view, on the bottom side of the picture) runs parallel to the horizontal. The left block is the one epoxyed on the guide while the right block is the one intended to move freely along the guide (refer to Figs. 4.2 & 4.18).
(**a**) Initial crack between the blocks at the beginning of experiment. Black spots alongside of the crack are metal power particles embedded into the wet epoxy-coating during the sample preparation process to serve as markers for monitoring relative displacements between the blocks.
(**b**) Vein with a tapered shape formed in the crack over a period of 46 days. Fibers are roughly normal to the vein instead of being parallel to the (horizontal) guide.
(**c**) View of the vein near the junction of the left block wit h the guide showing the broken ink-marked epoxy and gap (arrow) between the left block and the glass slide epoxyed on the guide, indicating at least a main part of the dilation across the vein was accommodated by fracturing and rotation of the left block from the guide.
(**d**) Another view of the same site in light of a different angle showing a new tapered vein of fibers (V) formed at the cracked junction of the left block with the guide.
(**e**) Photograph showing new fibrous veins developed in the fractured right block.
(**f**) Another photograph of new veins in the fractured right block.

(a)

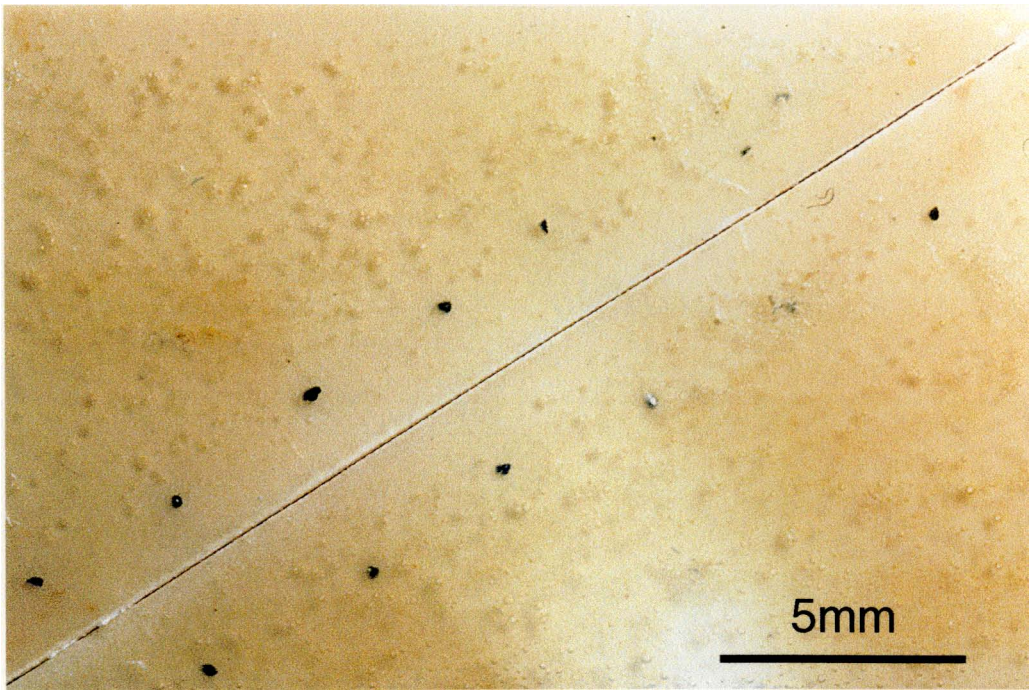

(b)

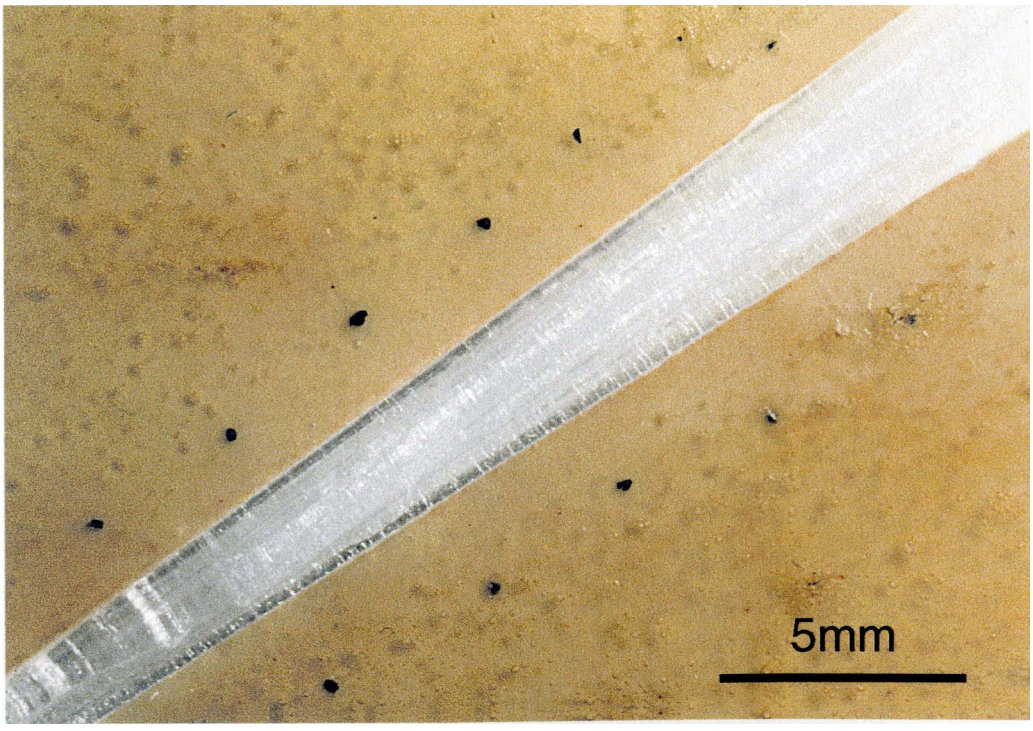

(c)

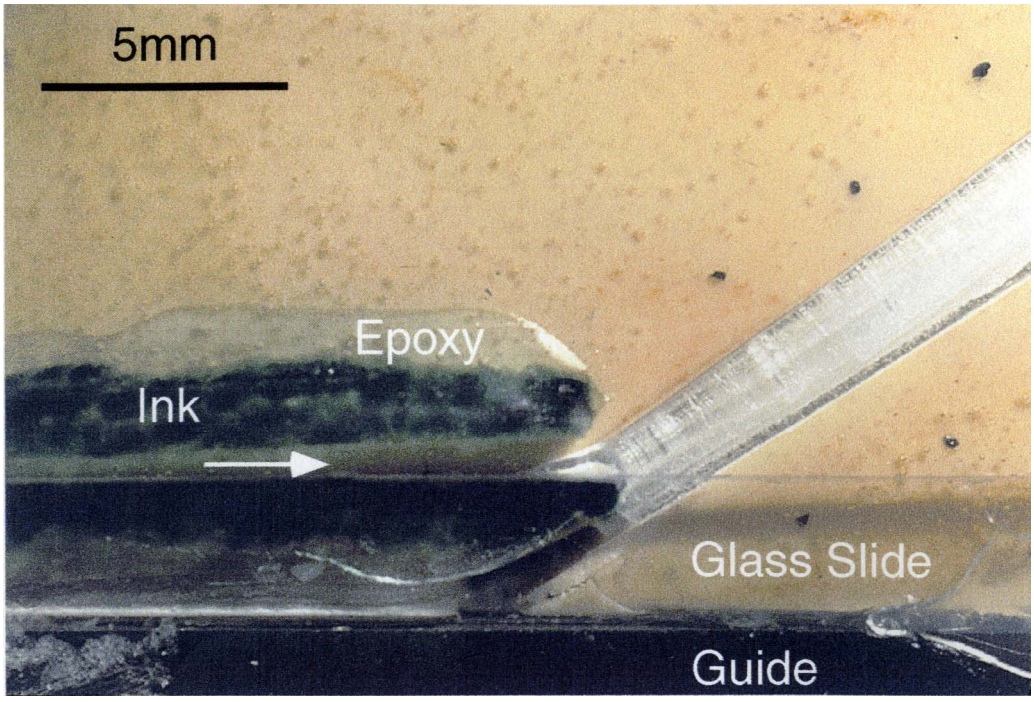

(d)

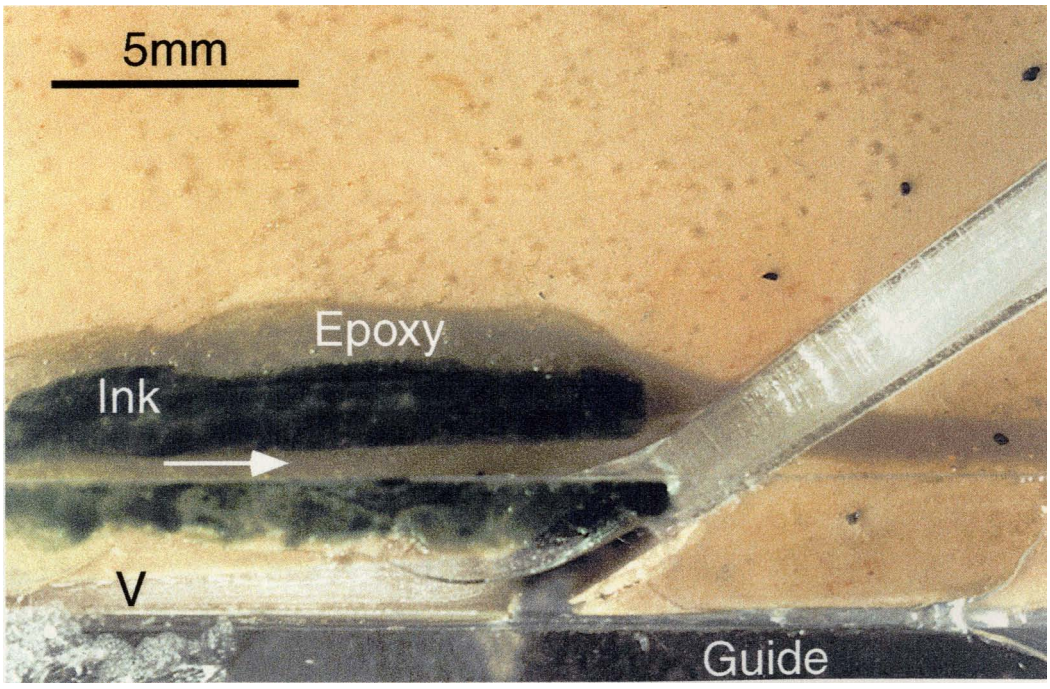

(e)

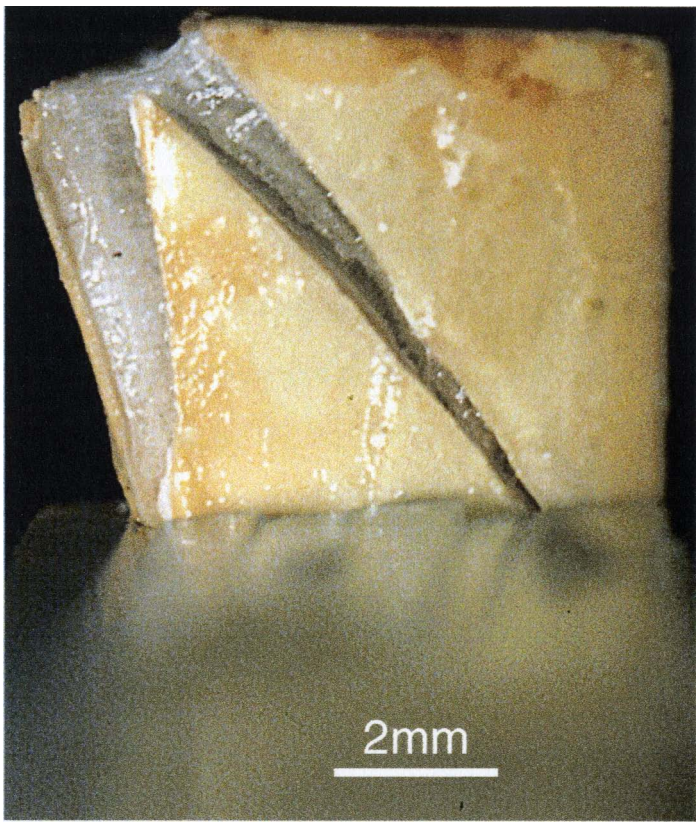

(f)

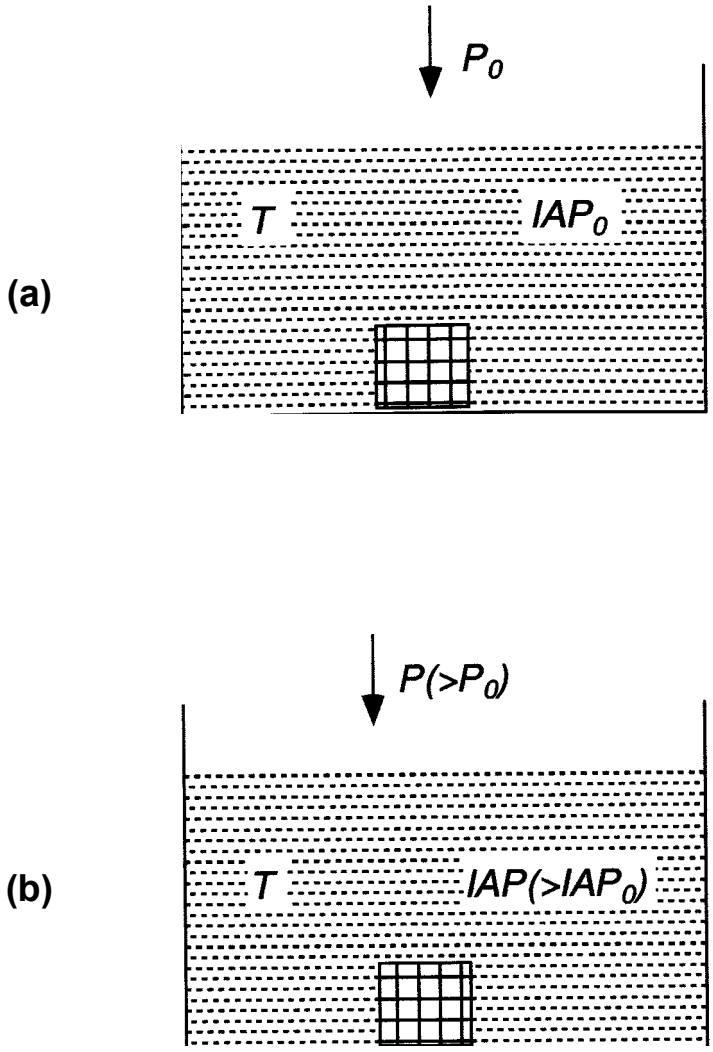

Fig. 5.1 Cartoons illustrating the general concept of the force of crystallization as interpreted by Weyl (1959), Maliva & Siever (1988a), and Wiltschko & Morse (1998). (**a**) When a solution has an equilibrium concentration, represented by $(IAP)_0$ (ionic activity product), under the given T and ambient pressure (P_0) conditions, crystal is neither growing nor dissolving. (**b**) When the solution is supersaturated $(IAP > IAP_0)$, crystal tends to grow and push against the ambient pressure and enclosing medium unless the ambient pressure is increased to a suitable level P that is exactly sufficiently large to stop the crystal growth and bring the system to new equilibrium. This maximum ambient pressure P or its increase $(P\text{-}P_0)$ is then interpreted as representing the ability of crystals to push aside the surrounding medium or the force of crystallization under the given supersaturation contions.

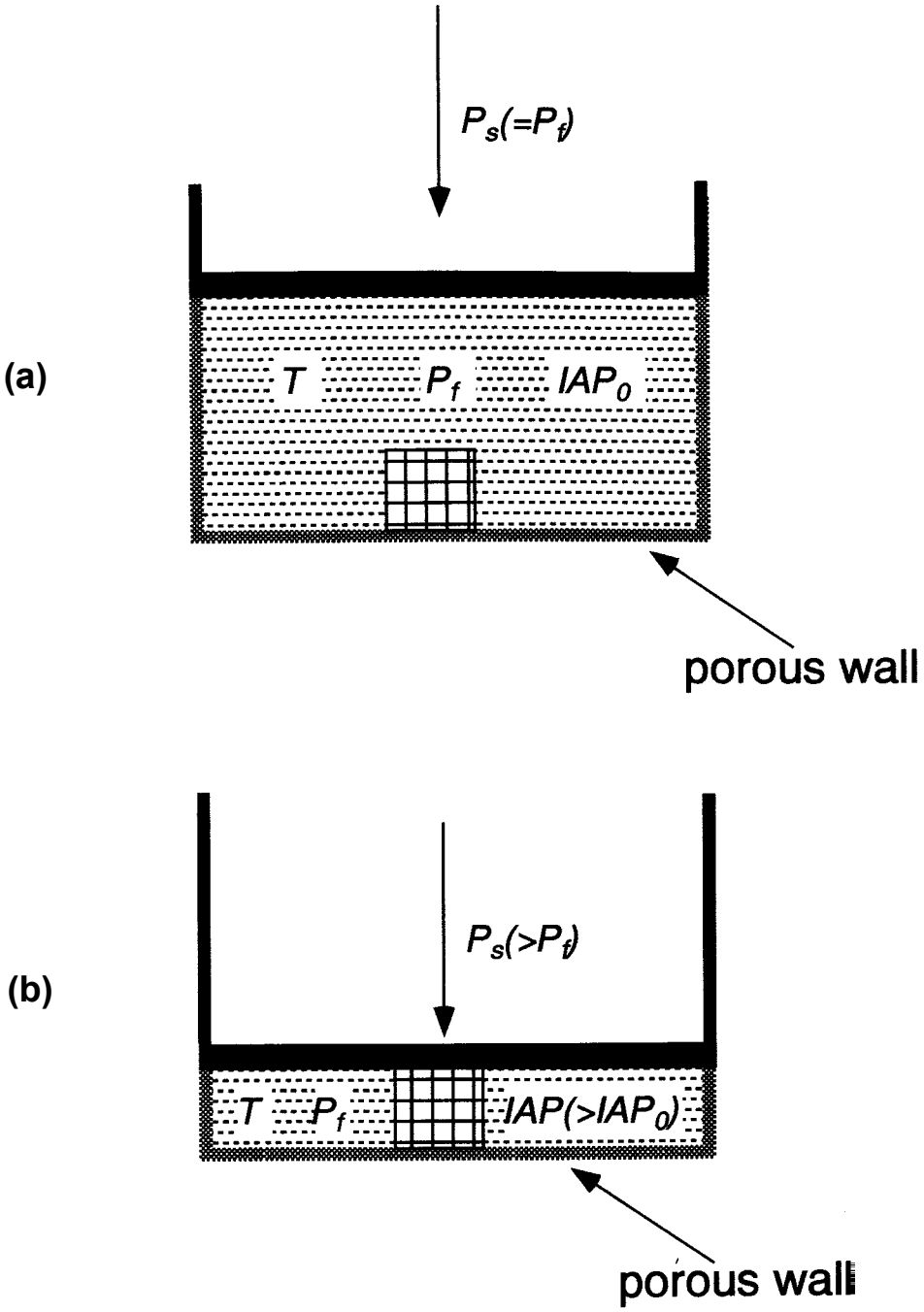

Fig. 5.2 Cartoons illustrating the proposed hypothetical model for the definition of the force of crystallization (Li & Means 1997). (a) When a solution has an equilibrium concentration, represented by $(IAP)_0$ (ionic activity product), under the given T and fluid pressure (P_f) conditions, crystal is neither growing nor dissolving. (b) When the solution is supersaturated $(IAP > IAP_0)$, crystal tends to grow and push against the piston with a higher pressure (P_s) than that of the fluid (P_f), unless P_s is increased to a suitable level that is suffciently large to stop the crystal growth and bring the system to new equilibrium. This maximum pressure difference $(P_s\text{-}P_f)$ is then interpreted as representing the ability of crystals to push aside the surrounding medium or the force of crystallization under the given supersaturation contions.

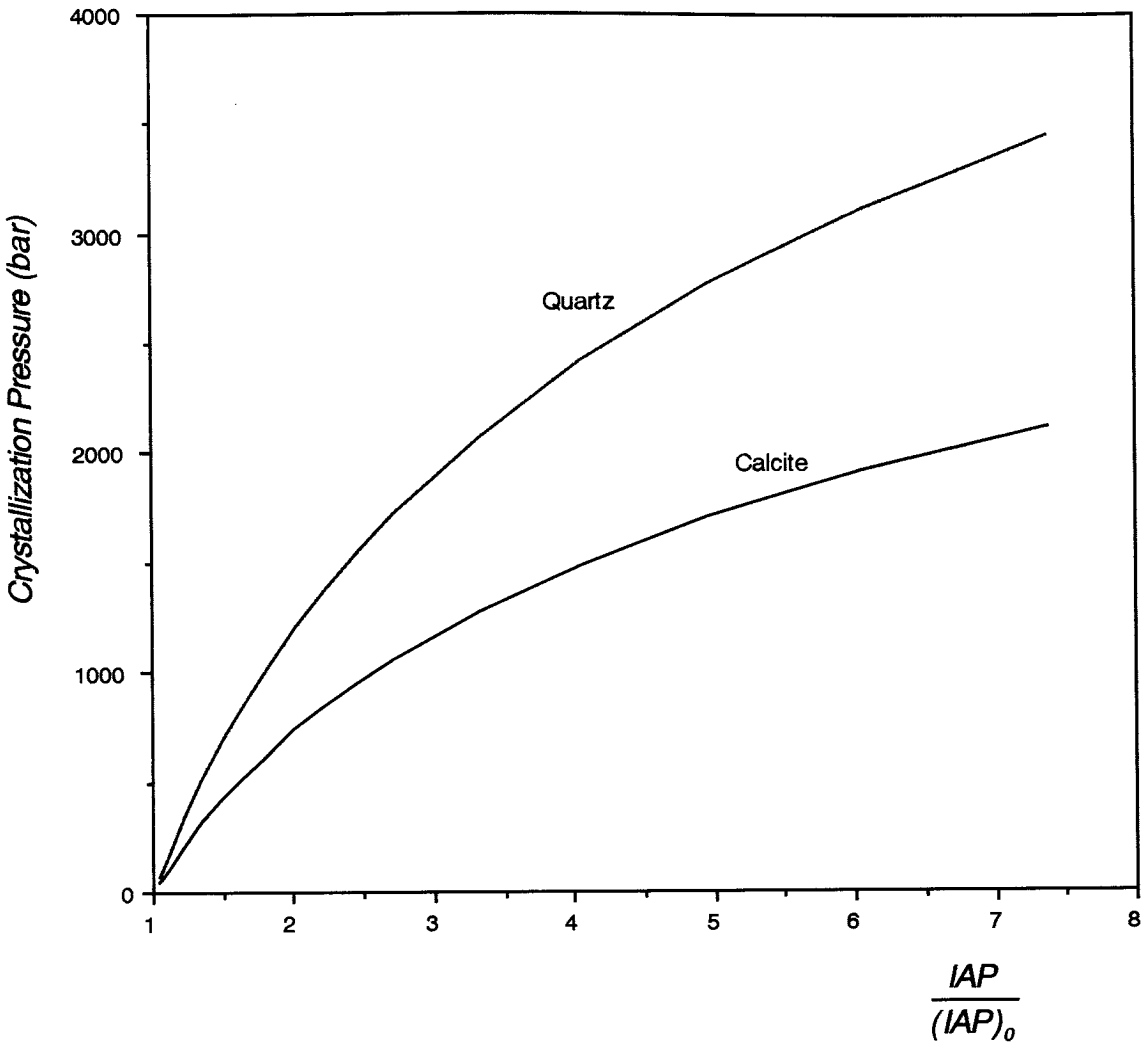

Fig. 5.3 Relationship between the crystallization pressure and supersaturation for quartz and calcite at 200°C plotted according to equation (6) (see also Table 5.1) (cf. Wiltschko & Morse 1998). The supersaturation degree is represented by $IAP/(IAP)_0$ where $(IAP)_0$ is the equilibrium ionic activity product of the solute with respect to a free crystal under the given T (=200°C) and P_f conditions while IAP is the actual ionic activity product at the same T and P_f conditions.

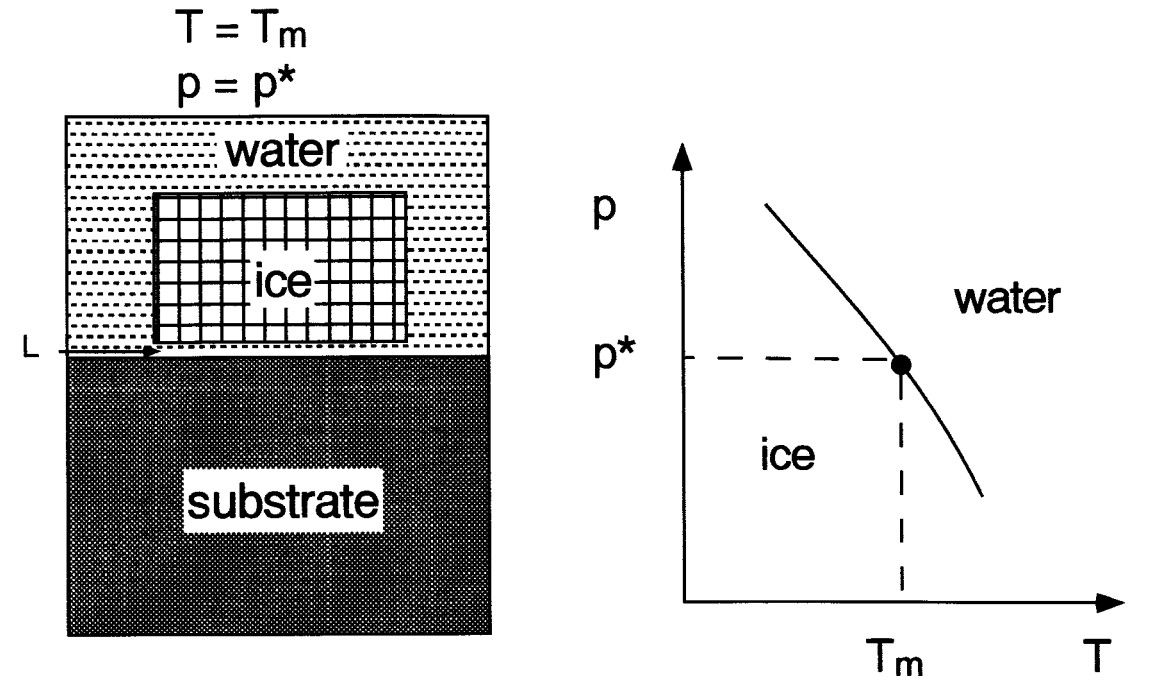

(a)

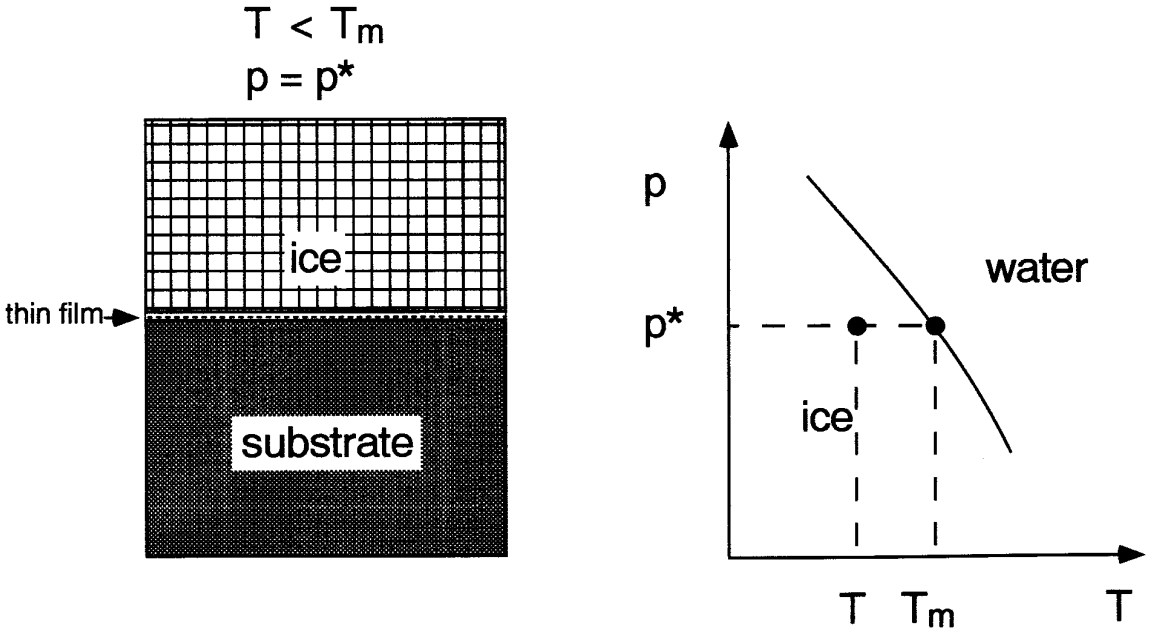

(b)

Fig. 5.4 Cartoons illustrating the phenomenon of surface melting in a one-component (H_2O) crystallization system. (a) When water is at equilibrium with the ice crystal at point (T_m, p^*), a macroscopic layer of liquid (L) exists between the crystal and the substrate. (b) When water is supercooled with respect to the bulk crystal at a temperature lower than T_m, at point (T, p^*), there still exists a microscopic thin film of supercooled liquid at the ice-substrate interface.

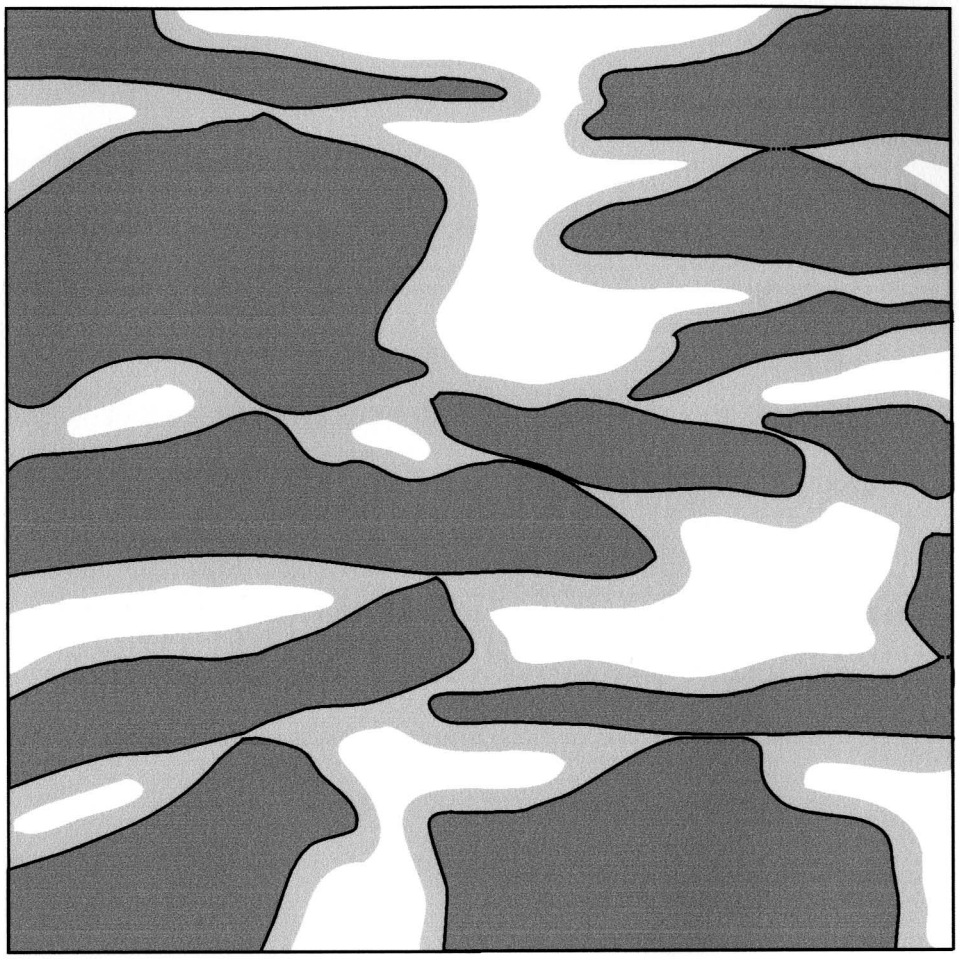

Fig. 5.5 Diagram of a cross section of a porous material partly saturated with a supersaturated crystallizing fluid, showing skeleton grains (dark areas), thin films of solution (light areas), and air spaces or crystals (white areas) (after Taylor & Ashcroft 1972, p. 8).

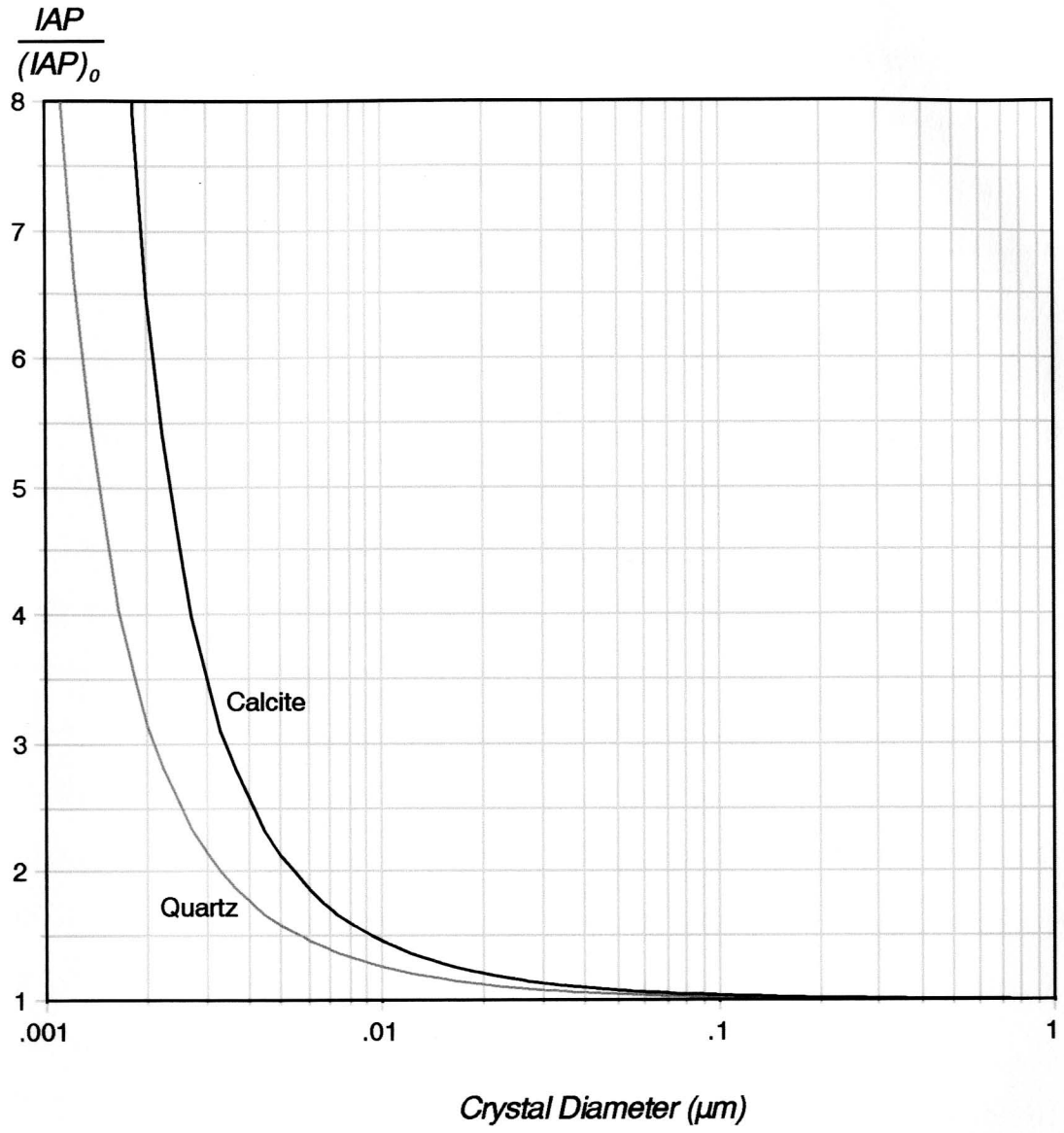

Fig. 5.6 Supersaturation levels of the crystallizing fluid at equilibrium with minute crystals of quartz and calcite at 200°C due to the Gibbs-Thomson effect, plotted according to equation (8) (see also Table 5.2). The supersaturation degree is represented by $IAP/(IAP)_0$ where $(IAP)_0$ is the equilibrium ionic activity product of the solute with respect to a bulk crystal under the given T (=200°C) and P conditions while IAP is the equilibrium ionic activity product with respect to a minute crystal at the same T and P conditions.

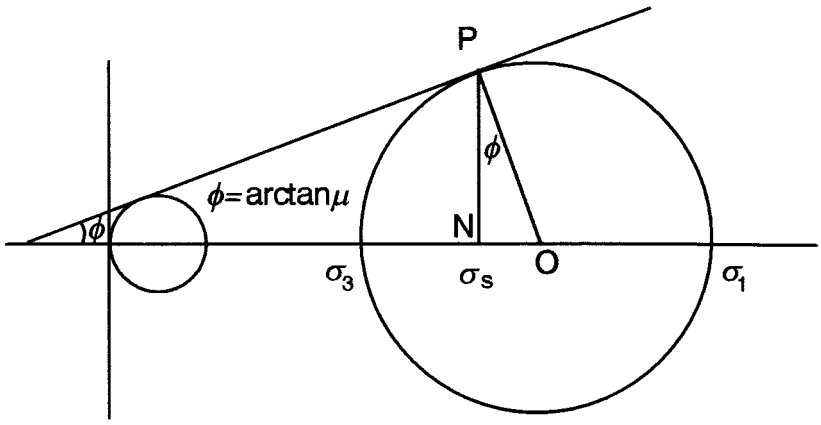

Fig. 5.7 Diagram showing how the compressive strength of a mineral or rock (σ_1-σ_3) increases with the confining pressure (σ_3). When σ_3=0, only a small Mohr circle (left) is required to touch the straight line Mohr envelope. When σ_3 increases, a larger Mohr circle (right) is required to touch the Mohr envelope.